JOURNAL OF GEOPHYSICAL RESEARCH, VOL. 101, NO. D23, PAGES 29,407–29,429, DECEMBER 27, 1996

A 6-year climatology of cloud occurrence frequency from Stratospheric Aerosol and Gas Experiment II observations (1985–1990)

Pi-Huan Wang,[1] Patrick Minnis,[2] M. Patrick McCormick,[3] Geoffrey S. Kent,[1] and Kristi M. Skeens[1]

Abstract. A 6-year climatology of subvisual and opaque cloud occurrence frequencies is established using observations from the Stratospheric Aerosol and Gas Experiment (SAGE) II between 1985 and 1990. The subvisual clouds are observed mostly at high altitudes near the tropopause. The opaque clouds terminate the profiling, reducing the measurement frequency of the SAGE II instrument in the troposphere. With its 1-km vertical resolution, the climatology shows many interesting features, including (1) the seasonal expansion and migration behavior of the subvisual and opaque cloud systems; (2) the association of the zonal mean cloud frequency distributions with the tropospheric mean circulation (Hadley and Ferrel cells); (3) the tropical cloud occurrence that follows the equatorial circulation, including the Walker circulation over the Pacific Ocean; and (4) the overall higher cloud occurrence in the northern hemisphere than in the southern hemisphere. The radiative impact of subvisual clouds is estimated to be a 1-W m^{-2} reduction in outgoing longwave radiation. The maximum overall effect is a net positive cloud forcing of 0.5–1 W m^{-2} in the tropics. During the 1987 El Niño-Southern Oscillation (ENSO), cloud frequency was generally enhanced in the tropics and mid-latitudes and reduced in the subtropics and high latitudes. The present study shows a distinct negative correlation between the high-altitude cloud occurrence and the lower stratospheric water vapor mixing ratio in the tropics, providing intrinsic evidence on the delicate connection between the stratospheric-tropospheric exchange and dehydration processes and the high-altitude cloud activities.

1. Introduction

Clouds play important roles in the hydrological cycle and climate of the Earth [e.g., *Chahine*, 1992; *Liou*, 1992; *Hobbs*, 1993]. They increase the global albedo, significantly reducing the absorption of solar radiation and the emission of longwave to space [e.g., *Ramanathan et al.*, 1989]. Clouds also change horizontal and vertical distributions of radiative heating with subsequent impacts on global circulation. A complete description of clouds is not a simple matter. It requires information on their location, size, duration, and occurrence frequency, as well as their optical properties, including particle size distribution, composition (or refractive index), and particle shape. A detailed set of such information is still far from complete. This is particularly the case for high-altitude thin cirrus clouds [*Sassen et al.*, 1990; *Gayet*, 1992]. Considerable efforts have been devoted to understanding the behavior of clouds in recent years. Research programs such as the International Satellite Cloud Climatology Project (ISCCP) [*Schiffer and Rossow*, 1985; *Rossow and Schiffer*, 1991], the First International Satellite Cloud Climatology Project Regional Experiment (FIRE) [*Cox et al.*, 1987], the Experimental Cloud Lidar Pilot Study (ECLIPS) [*World Meteorological Organization*, 1988; *Platt et al.*, 1994], and the International Cloud Experiment (ICE) [*Ansmann et al.*, 1991] have been put forth with great effort to improve the information on cloud systems. In addition, information on the global distribution of total cloud cover and amounts of cloud types have recently become available [*Warren et al.*, 1986, 1988; *Stowe et al.*, 1989; *Rossow and Schiffer*, 1991; *Wylie et al.*, 1994]. The objective of this study is to develop a new climatology of cloud occurrence frequency based on the solar occultation observations of the Stratospheric Aerosol and Gas Experiment (SAGE) II.

The SAGE II observations have provided new cloud information in recent years [e.g., *Wang et al.*, 1994a; *Liao et al.*, 1995a, b; *Kent et al.*, 1995a; *Wang et al.*, 1995a]. *Woodbury and McCormick* [1983] first used a simple method to identify cloud events to study cloud distributions based on SAGE I data [see also *Woodbury and McCormick*, 1986]. Later, this method was employed by *Chiou et al.* [1990] to investigate cloud statistics using SAGE II measurements. Generally, clouds sensed by the SAGE II instrument can be grouped into two categories according to the 1-μm extinction

[1]Science and Technology Corporation, Hampton, Virginia.
[2]Atmospheric Sciences Division, NASA Langley Research Center, Hampton, Virginia.
[3]Hampton University, Hampton, Virginia.

Paper number 96JD01780.
0148-0227/96/96JD-01780$09.00

coefficient of the observed clouds. The first category classifies clouds having extinction coefficients within the measurement limit of the SAGE II instrument. The second category classifies clouds having extinction coefficients beyond the instrument measurement limit. The present study combines the techniques for detecting both types of clouds and applies them to the series of SAGE II observations. In this presentation, the features of the SAGE II instrument relevant to cloud detection are described in section 2. The definition of SAGE II cloud parameters is discussed in section 3, followed by an analysis of the cloud frequency climatology in section 4. Section 5 is devoted to discussion. A summary is presented in section 6.

2. Relevant Features of SAGE II

The SAGE II instrument is a seven-channel radiometer. It uses the solar occultation technique to provide two measurements per orbit, one during spacecraft sunrise (when the satellite instrument emerges from the dark side to the sunlit side of the orbit) and another during sunset (when the instrument enters the dark side from the sunlit side of the orbit). These seven channels are centered at 0.385-, 0.448-, 0.453-, 0.525-, 0.600-, 0.940-, and 1.02-μm wavelengths. The Earth limb transmission measurements from these channels are used to determine the vertical profile of stratospheric ozone, nitrogen dioxide, water vapor, and the aerosol extinction coefficient at 0.385-, 0.453-, 0.525-, and 1.02-μm wavelengths. Under favorable atmospheric conditions such as nonvolcanic, cloud free, and optically thin clouds, measurements from channels at the four longer wavelengths also provide tropospheric data, especially the 1.02-μm channel (due to the lower relative molecular attenuation at these wavelengths) [*Kent et al.*, 1995b]. The SAGE II sensor aboard the Earth Radiation Budget Satellite (ERBS) has been operating since October 1984. The orbital characteristics of ERBS are such that the SAGE II sunrise measurements provide a latitudinal coverage of approximately 135° in about 1 month. The two latitudinal extremes of the measurements vary with the season. With a 90-min orbiting period, the 15 SAGE II daily sunrise measurements are distributed almost evenly in longitude, with a small latitudinal shift between successive events. These sampling features are also true for the SAGE II sunset measurements. Poleward of about 55°N–55°S, no samplings are available during the boreal/austral winter. The field of view of the instrument is specified by a coverage of 0.5 km (in the vertical) by 2.5 km (in the horizontal) at the limb tangent point. By assuming a spherically symmetric atmosphere, the SAGE II retrieval process generates spatially smoothed data characterized by a volume with a height of 1 km, a width of 2.5 km, and a length of about 200 km. *Mauldin et al.* [1985] and *McCormick* [1987] describe the SAGE II measurement characteristics, while *Chu et al.* [1989] detail the SAGE II data inversion process. *Wang et al.* [1994a] have discussed in detail the constraints on the SAGE II cloud observations.

The schematic diagram (Figure 1) of the 1-μm extinction coefficient measurement range of the instrument illustrates the characteristics of the SAGE II cloud detection. The upper measurement limit of the SAGE II extinction coefficient (1.02 μm) is about 2 X 10^{-2} km^{-1}. Under nonvolcanic conditions (e.g., 1989), the level of aerosol extinction coefficients is about 2 X 10^{-4} km^{-1}. Thus clouds with extinction coefficients between 2 X 10^{-4} km^{-1} and 2 X 10^{-2} km^{-1} are measurable by the SAGE II sensor. For clouds having extinction coefficients greater than the SAGE II measurement limit, the transmitted signals drop below the SAGE II sensitivity threshold, resulting in termination of the cloud profile at an altitude corresponding to this upper limit. These clouds are referred to as SAGE II opaque clouds. Figure 1 also displays the cirrus cloud classification of *Sassen and Cho* [1992] in terms of cloud optical depth at about 0.7-μm wavelength. Note that the extinction scale in Figure 1 is approximately the optical depth scale for 1-km-thick clouds. Therefore, according to their cirrus cloud classification, SAGE II opaque clouds generally include all types of clouds (having optical depth greater than ~0.02), and the SAGE II measurable clouds correspond mostly to the subvisual cirrus clouds [*Wang et al.*, 1994a]. Note that the class of thin cirrus clouds of *Sassen and Cho* [1992] is shown as part of the SAGE II opaque cloud category (Figure 1). Clearly, the presence of SAGE II opaque clouds reduces the measurement opportunities of the SAGE II instrument in the troposphere [*Wang*, 1994].

The eruption of Mount Pinatubo (15.14°N, 120.35°E) in the Philippines on June 15, 1991, produced the largest volcanic impact to the stratosphere ever observed by satellite instruments [*McCormick*, 1992]. The greatly enhanced aerosol loadings immediately following the eruption prohibited the SAGE II instrument from reaching below an altitude of about 20 km during the first several months after the eruption [*McCormick et al.*, 1993]. This condition is improving slowly with time [*Wang et al.*, 1994b], and therefore the present work

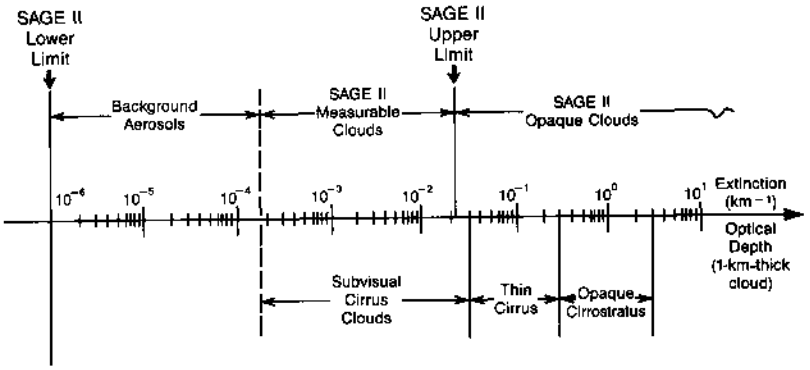

Figure 1. The measurement range of the SAGE II 1-μm particulate extinction coefficient. The classification of cirrus clouds is based on *Sassen and Cho* [1992].

of a cloud climatology includes the 6-year SAGE II observations prior to the eruption, from 1985 to 1990. The analysis of subvisual clouds and the analysis of opaque clouds will be treated separately in the present investigation.

3. Definition

The definition of the opaque cloud frequency has been given by *Wang et al.* [1995b] in detail. We will summarize their analysis method and extend the investigation to subvisual clouds. Let N_t be the total number of SAGE II overpasses within a given geographical area during a certain time period and $N_m(z)$ be the number of measurable events that occurred in a 1-km-thick SAGE II layer centered at an altitude of z. Because only these measurement events $N_m(z)$ at z are able to reach the next lower layer centered at $z - 1$, a general relationship between the number of measurements at two adjacent arbitrary layers can be summarized in the expression

$$N_m(z) = N(z-1) = N_m(z-1) + N_c^o(z-1) \quad (1)$$

where $N(z-1)$ indicates the total number of SAGE II samples that occurred in the layer centered at $z - 1$, and $N_m(z-1)$ and $N_c^o(z-1)$ are the number of SAGE II measurable and opaque cloud events, respectively, that occurred in the same layer. The upper boundary condition is simply given by $N_t = N(z) = N_m(z) + N_c^o(z)$ at the highest layer where SAGE II observations encountered opaque cloud(s). These measurable events $N_m(z-1)$ can be further divided into aerosol measurements $N_a(z-1)$ and subvisual cloud events $N_c^s(z-1)$. Therefore we have

$$N_m(z) = N(z-1) = N_a(z-1) + N_c^s(z-1) + N_c^o(z-1) \quad (2)$$

The occurrence frequency of the SAGE II subvisual and opaque clouds at an altitude z can be defined as

$$f^s(z) = \frac{N_c^s(z)}{N(z)} \times 100\% \quad (3)$$

and

$$f^o(z) = \frac{N_c^o(z)}{N(z)} \times 100\% \quad (4)$$

respectively, because there are $N_c^s(z)$ subvisual cloud events and $N_c^o(z)$ opaque cloud events in the total number of $N(z)$ samples occurring at the layer centered at z. The total cloud frequency is simply given by the sum of $f^s(z)$ and $f^o(z)$. *Wang et al.* [1995b] have also discussed the upper and lower bounds of the frequency estimate according to the assumptions of measurable clouds or opaque clouds for the portion of the total SAGE II overpasses (N_t) that failed to reach the layer centered at z owing to the presence of opaque clouds at higher altitudes. Similar upper and lower bounds can also be formulated for the subvisual clouds based on these assumptions.

The 1-μm extinction coefficient that separates aerosols and subvisual clouds (Figure 1) depends on the aerosol loading in the atmosphere. Unfortunately, the atmospheric aerosol loading exhibits significant spatial and temporal variabilities, particularly after volcanic eruptions [e.g., *Kent et al.*, 1995b]. For this reason, the suitability of using a single extinction coefficient as a reference to distinguish clouds from aerosols is questionable. Recently, a new method was developed for separating aerosols from clouds based on SAGE II extinction coefficient measurements at 0.525 and 1.02 μm [*Kent et al.*, 1993]. Because the ratio of extinction coefficients at two different wavelengths contains information on particle size, the usage of SAGE II measurements at 0.525 and 1.02 μm strengthens the ability to separate aerosol and cloud data. Because the 0.525-μm SAGE II measurements do not reach below 6.5 km due to strong Rayleigh attenuation, the subvisual cloud analysis in the present study is limited to altitudes above 6.5 km.

A comparison between the 1986 SAGE II opaque cloud observations and the 1952–1981 cloud climatology of *Warren et al.* [1986, 1988] showed an agreement within 20% in the tropics, with the mean SAGE II frequency greater than the surface observation [*Wang et al.*, 1995b]. In that study, the 1986 SAGE II data were integrated to match the vertical resolution of the 1952–1981 climatology. Because the SAGE II analysis counts the cloud of a given layer independently, it is possible that a cloud may have been counted more than once if the depth of the cloud covers more than one contiguous layer. Although it is possible for the surface observation to miss the occurrence of high- and middle-level clouds when low-level overcast is present, the surface analysis attempts to account for higher clouds in low overcast conditions using a best estimate technique [*Warren et al.*, 1986]. The occurrence frequencies in the SAGE II and surface data sets may also differ because of discrepancies in the year and times of day that were sampled and because of differences in the field of view (horizontal resolution). The SAGE II observations may have a smaller probability of seeing a given cloud than a surface observer due to the satellite instrument's 2.5 X 200 (km^2) horizontal resolution as compared with the resolution of a diameter of 45–90 km of a surface observer [*Warren et al.*, 1988].

4. Results

In order to infer the 6-year zonal mean cloud frequency distribution, the SAGE II data are binned into 10° latitudinal bins centered at −70°, −60°, and so forth up to 70°. To examine the seasonal behavior of the cloud frequency distributions, the 6-year SAGE II data are further grouped according to season in the zonal mean distribution analysis. To investigate the zonal variability to cloud occurrence, SAGE II data are grouped into bins of size 10° latitude by 24° longitude. The 24° increment in longitude matches the longitudinal separation of two adjacent SAGE II samples. To study the cloud temporal variations, time series of the occurrence are constructed from seasons of individual years from 1985 to 1990. Because the data acquisition of the SAGE II instrument includes two specific modes, the sunrise and the sunset samplings, the differences in cloud frequency between sunrise and sunset observations are examined.

4.1 Zonal Mean Distributions

The 6-year zonal mean distributions of cloud occurrence frequency of the SAGE II subvisual and opaque clouds are displayed in Figure 2. Subvisual clouds (SVCs) occur most often just below the tropopause. A maximum in the mean frequency distribution of about 45% is found at 15 km near the equator. At middle and high latitudes, the SVCs reveal a range

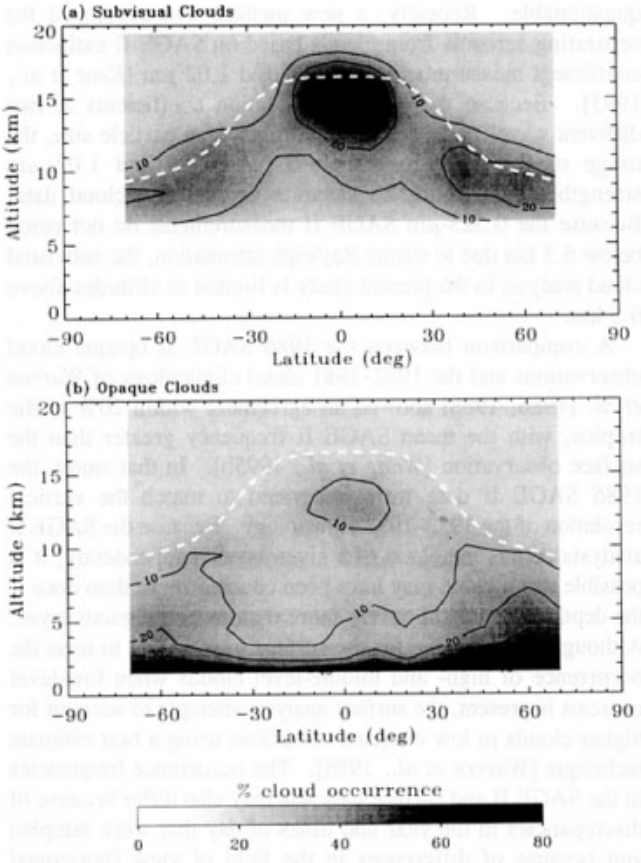

Figure 2. Six-year averaged zonal mean distribution of the SAGE II (a) subvisual and (b) opaque cloud occurrence frequency. The dashed lines indicate the tropopause.

of frequency up to about 20%. The SVCs appear slightly more often at the northern midlatitudes than at the southern midlatitudes. The occurrence of SVCs extends to about 3 km above the mean tropopause altitude in the tropics and at the middle and high latitudes.

The vertical distribution of the SAGE II opaque clouds (OC) is quite different. The frequency decreases generally as altitude increases, except in the tropics where the frequency shows a local maximum of about 15% at an altitude of 13 km. The OC occurrence is less than 5% above the tropopause. Latitudinally, the distribution shows three favorable major regions for OC development. One is located near the equator, and the other two are high latitudes centered at about 60°N and 60°S. The results also show higher cloud frequency in the northern hemisphere than in the southern hemisphere. While the cloud system in the tropics is related to the deep convective activities in the Intertropical Convergence Zone (ITCZ) the cloud occurrence at the middle and high latitudes is presumably associated with frontal systems, especially in the northern hemisphere. The 1952–1981 cloud climatology of *Warren et al.* [1986, 1988] indicates that cirrus and stratus clouds are the main components at northern high latitudes. The former cloud type occurs most often near 60°N, while the latter peaks near 75°N during sunlit months [*Warren et al.*, 1986, 1988]. In the subtropical regions above about 4 km, the mean distributions show relatively infrequent (<10%) OC occurrence. Diminished SVC frequency is also evident in the same subtropical regions. These subtropical regions are known for intrusion of dry air from the stratosphere. They correspond well with regions of low atmospheric humidity [e.g., *Manabe et al.*, 1965; *Von de Berg et al.*, 1991]. In general, the distribution of the zonal mean frequency in Figure 2 is consistent with the tropospheric mean circulation (Hadley and Ferrel cells) [see also *Wang*, 1994]. In the mixing layer at altitudes below about 3–4 km, Figure 2 shows high frequency of the SAGE II OCs, up to 50–70%.

4.2 Seasonally Averaged Zonal Mean Distributions

By grouping the 6-year SAGE II data according to season, the seasonal variations of zonal mean cloud occurrence may be examined. As shown in Figure 3, the tropical maximum in both types of SAGE II clouds moves from about 5°N in March–April–May (MAM) to about 10°N in June–July–August (JJA). This cloud maximum remains more or less at 10°N during September–October–November (SON), followed by shifting to about 5°S in December–January–February (DJF). The latitudinal movements of the tropical maxima are in concert with the seasonal shift of the ITCZ. The cloud occurrence in the subtropical regions also has a distinct seasonal variation, with the maximum frequency in local summer and the minimum during local winter. Similar seasonal features can be found in the cloud climatologies based on surface observations [*Warren et al.*, 1986, Figure 7; 1988, Figure 11], Nimbus 7 cloud data [*Stowe et al.*, 1989, Figures 16 and 17], and data from the high-resolution infrared radiation sounder (HIRS) [*Wylie et al.*, 1994, Figure 2]. This subtropical seasonal variation is particularly clear for the SAGE II opaque clouds and is indicative of enhanced descending air motion in the subtropics during winter, consistent with the seasonal behavior of the stratosphere-troposphere exchange processes inferred from lidar backscatter measurements [*Menzies and Tratt*, 1995]. Because there are no data poleward of about 55° during local winter, the results of the 6-year zonal average at high latitudes above 55° (Figure 2) will be slightly biased toward the summer season. Note that elevated land surfaces contribute to the more frequent low clouds in the northern midlatitudes compared with the southern midlatitudes, owing to the relative proportions of land and ocean in the two hemispheres. Clear skies over higher-altitude land surface may be mistaken as low clouds. Because the results in Figure 2 are zonally averaged quantities, the surface influence on the mean cloud frequency should be minimal.

4.3 Longitudinal Variations

The altitude-longitude distributions of the 6-year mean cloud occurrence are displayed in Figure 4. In the tropics, clouds occur most often over the western Pacific Ocean, Micronesia, central Africa, and the northern part of South America. The maximum (~70%) occurrence frequency for SVC is located at an altitude of 15.5 km over Micronesia. A peak in the OC frequency of about 40% is shown near 12.5 km over the same area. The OC frequency is less than 5% at altitudes above about 5 km over the eastern Pacific Ocean. The SVC frequency is also minimal in this region. The longitudinal distributions in the tropics are generally consistent with the cloud pattern associated with the equatorial circulation, including the so-called Walker circulation over the tropical Pacific Ocean [*Peixoto and Oort*, 1992; *Wang*, 1994].

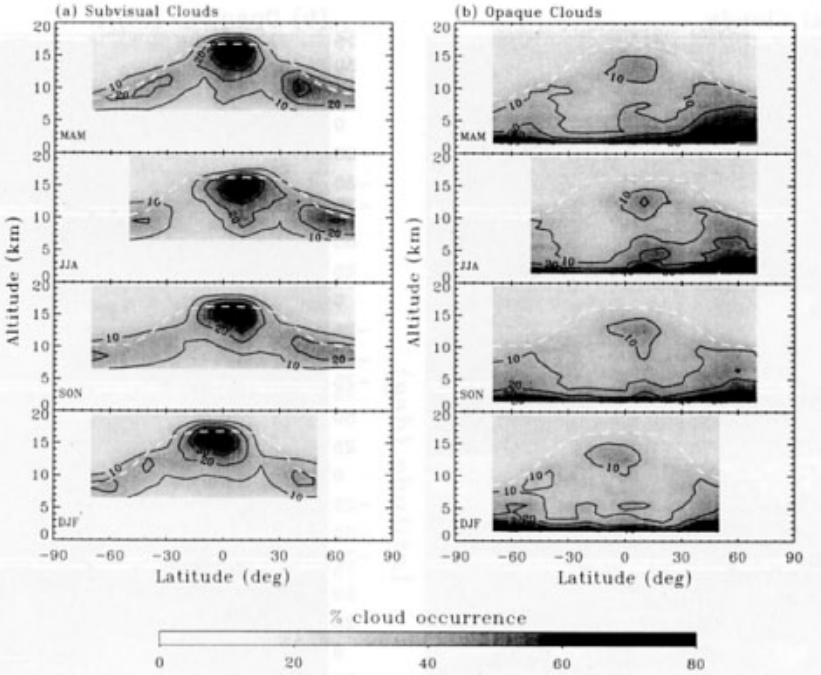

Figure 3. Six-year seasonally averaged zonal mean distribution of the SAGE II (a) subvisual and (b) opaque cloud occurrence frequency. The dashed lines indicate the tropopause.

At 20°N, the results show OC frequencies as great as 10% in the upper troposphere over South China, northern Africa, and the eastern Pacific Ocean and Mexico. Over these regions, the SVC frequency is about 20–30%. At 20°S, the occurrence of OCs is generally less than 5%, except over central South America and the central Pacific Ocean. SVC occurrence is more frequent, over 20%, in these longitudinal sectors than in the others. In the midlatitudinal storm belts (50°S and 50°N), the longitudinal distributions are relatively uniform compared with those in the tropical and subtropical regions. Comparatively, the cloud occurrence distribution at the northern midlatitudes reveals more longitudinal structure than that in the southern midlatitudes. At 50°N, the results below an altitude of about 7 km show generally higher OC frequencies between 140°E and 360°E than from 0°E to 140°E. This feature may be related to the ocean-land geography in the midlatitudinal

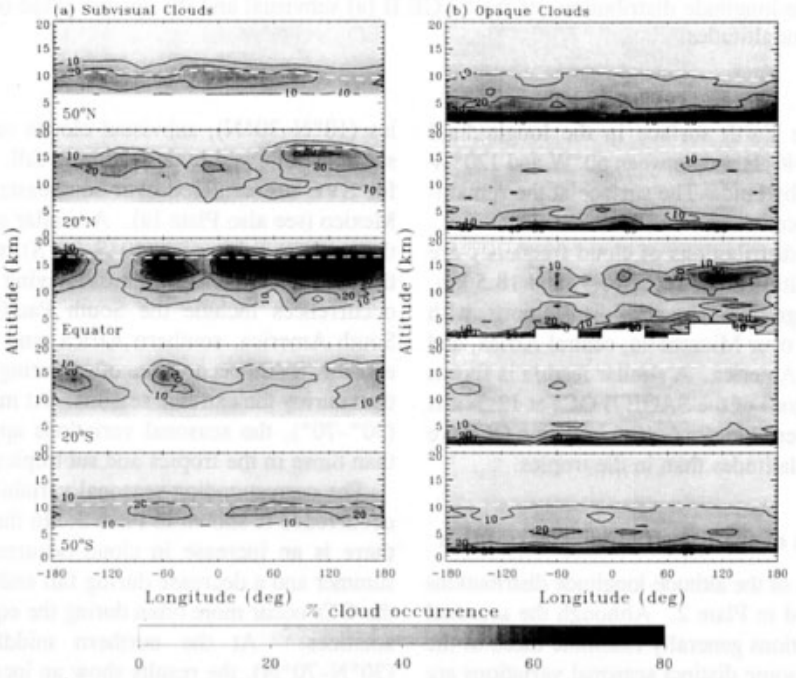

Figure 4. Altitude-longitude distributions of the SAGE II (a) subvisual and (b) opaque cloud occurrence frequency at different latitudes. The dashed lines indicate the tropopause.

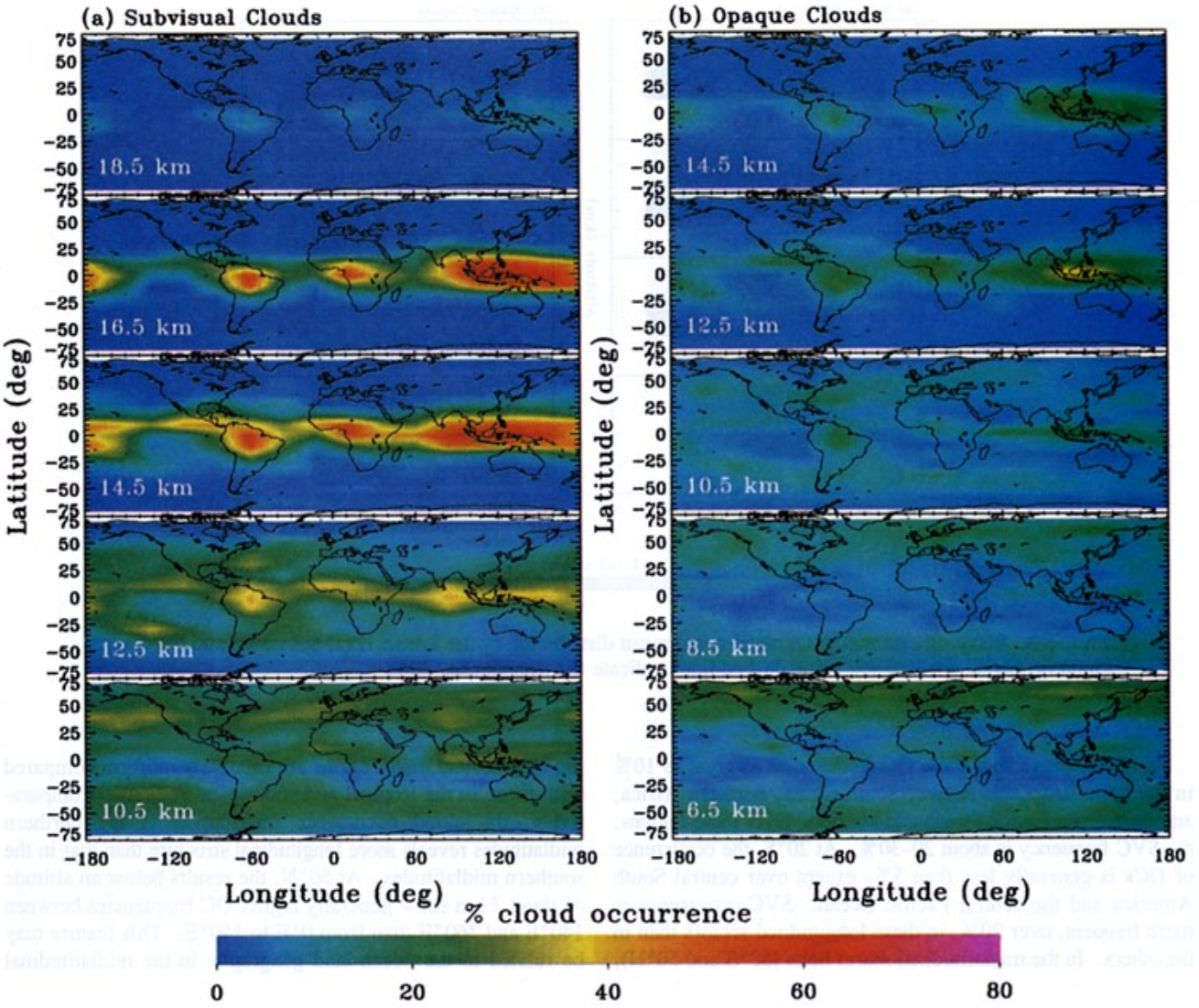

Plate 1. Latitude-longitude distributions of the SAGE II (a) subvisual and (b) opaque cloud occurrence frequency at different altitudes.

region. Near 50°N, the Earth surface in the longitudinal sectors between 0°E and 140°E and between 60°W and 120°W is covered almost entirely by land. The surface at the remaining longitudes is mostly ocean.

The latitude-longitude distributions of cloud frequency are presented in Plate 1. At altitudes of 14.5, 16.5, and 18.5 km, SVCs show organized geographic frequency distributions, with the local maxima centered over Micronesia, central Africa, and the northern part of South America. A similar feature is shown in the geographic distributions of the SAGE II OCs at 12.5- and 14.5-km altitudes. At lower altitudes (≤10.5 km), the OCs are more abundant in the midlatitudes than in the tropics.

4.4 Seasonal Variations of the Longitudinal Distribution

The seasonal variations of the altitude-longitude distributions of the SVCs are presented in Plate 2. Although the seasonal mean longitudinal distributions generally resemble those of the 6-year mean (Figure 4a), some distinct seasonal variations are evident, particularly in the subtropics. In the northern subtropics (10°N–30°N), subvisual clouds occur most often during summer followed by a decline in fall. The favored locations for SVC are centered over southeastern Asia and India, and Mexico (see also Plate 1a). A similar seasonal cycle occurs in the southern subtropics (10°S–30°S), with a maximum during the austral summer. The areas having the most frequent SVC occurrences include the South Pacific Convergence Zone, South America, southern Africa, and Australia. Around the equator, SVCs occur more often during the transitional seasons than during the extreme seasons. At middle and high latitudes (30°–70°), the seasonal variations appear to be less intense than those in the tropics and subtropics.

The corresponding seasonal variability in the SAGE II OC occurrence is shown in Plate 3. In the subtropics (10°–30°), there is an increase in cloud occurrence during spring and summer and a decrease during fall and winter. In the tropics, the OCs occur more often during the equinoxes than during the solstices. At the northern middle and high latitudes (30°N–70°N), the results show an increase in OC occurrence below about 8 km from winter to spring. During summer when

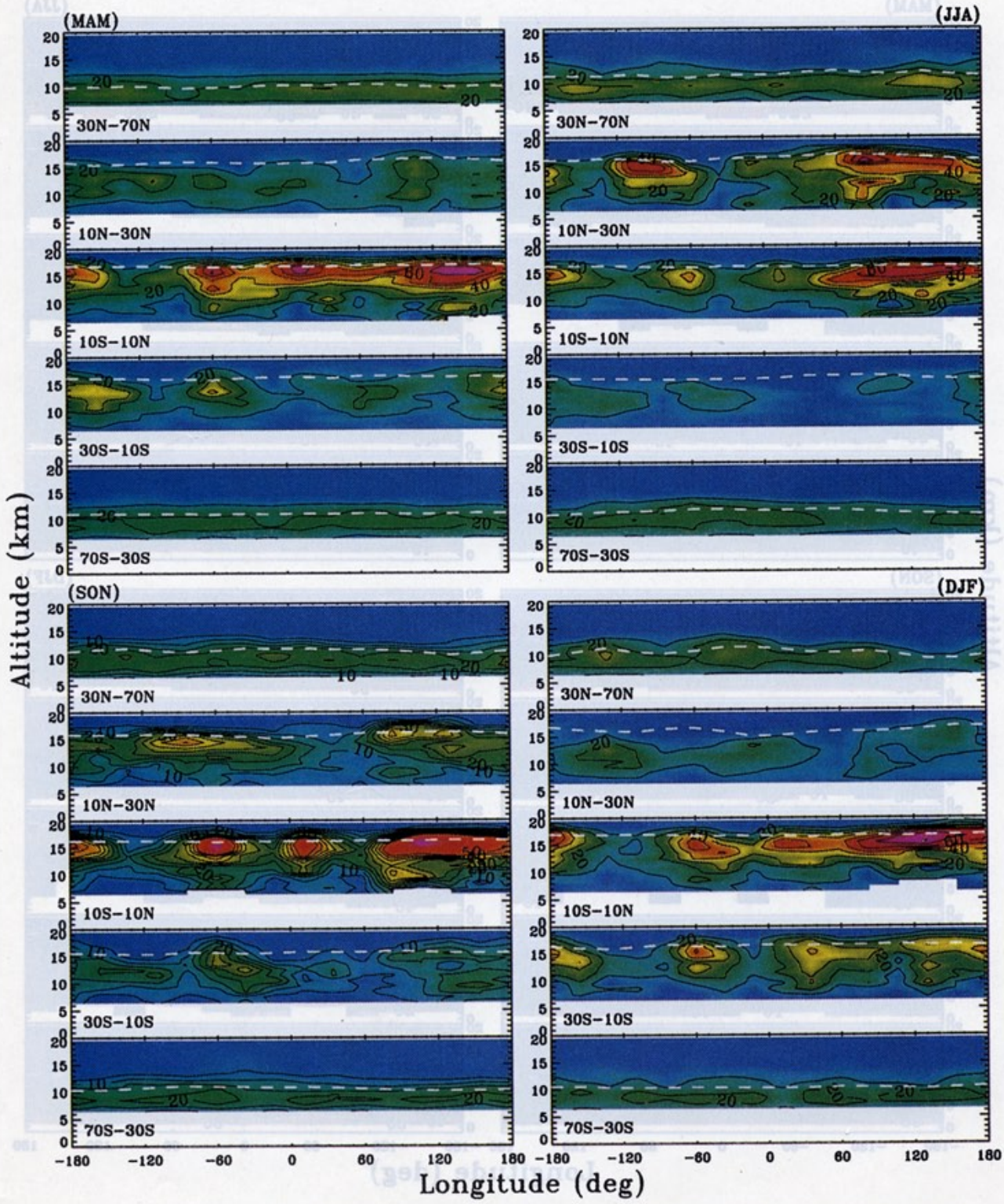

Plate 2. Seasonal variations of the altitude-longitude distributions of the SAGE II subvisual cloud occurrence frequency at different latitudes. The dashed lines indicates the tropopause. The color scale is the same as in Figure 2.

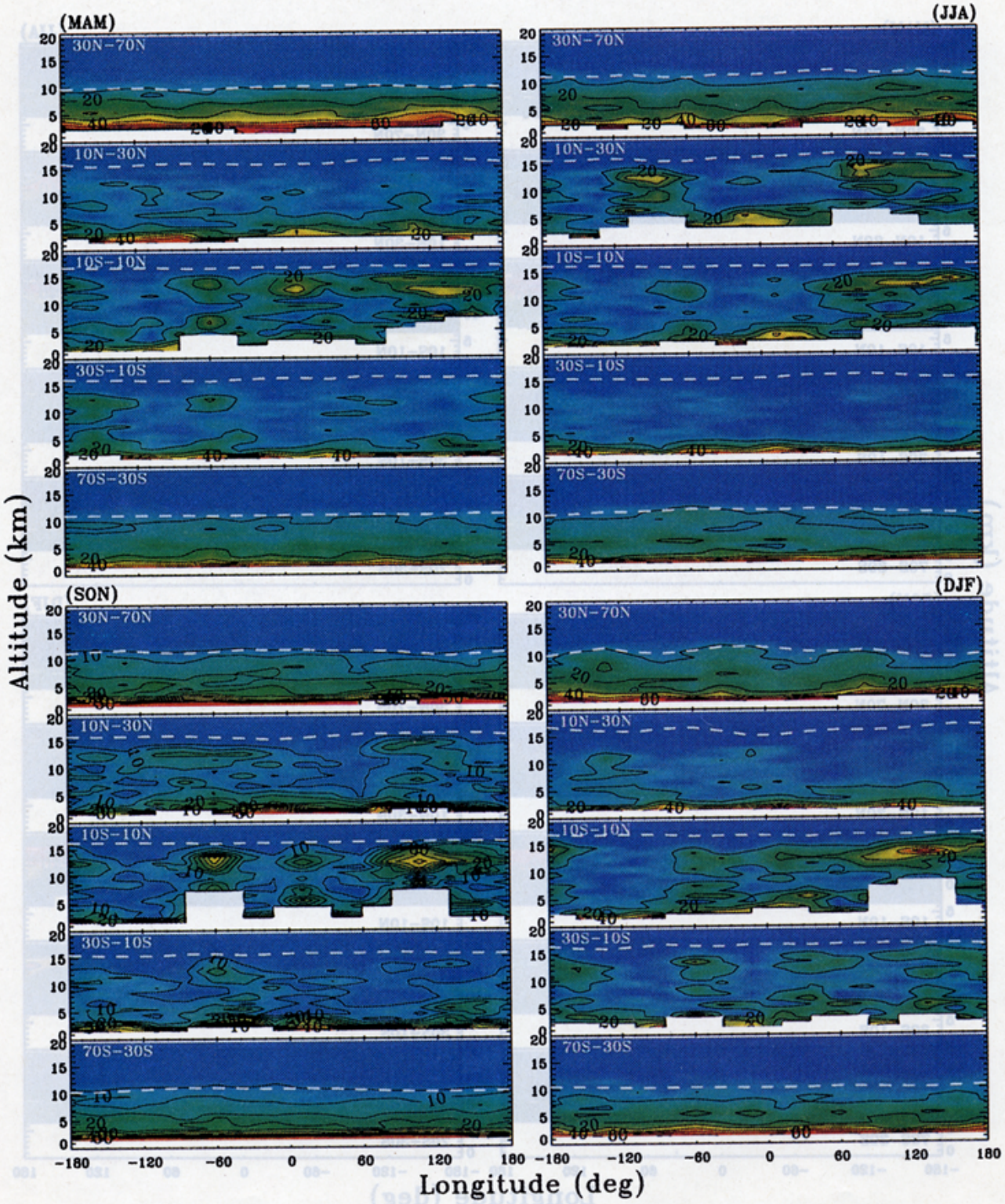

Plate 3. Seasonal variations of the altitude-longitude distributions of the SAGE II opaque cloud occurrence frequency at different latitudes. The dashed lines indicates the tropopause. The color scale is the same as in Figure 2.

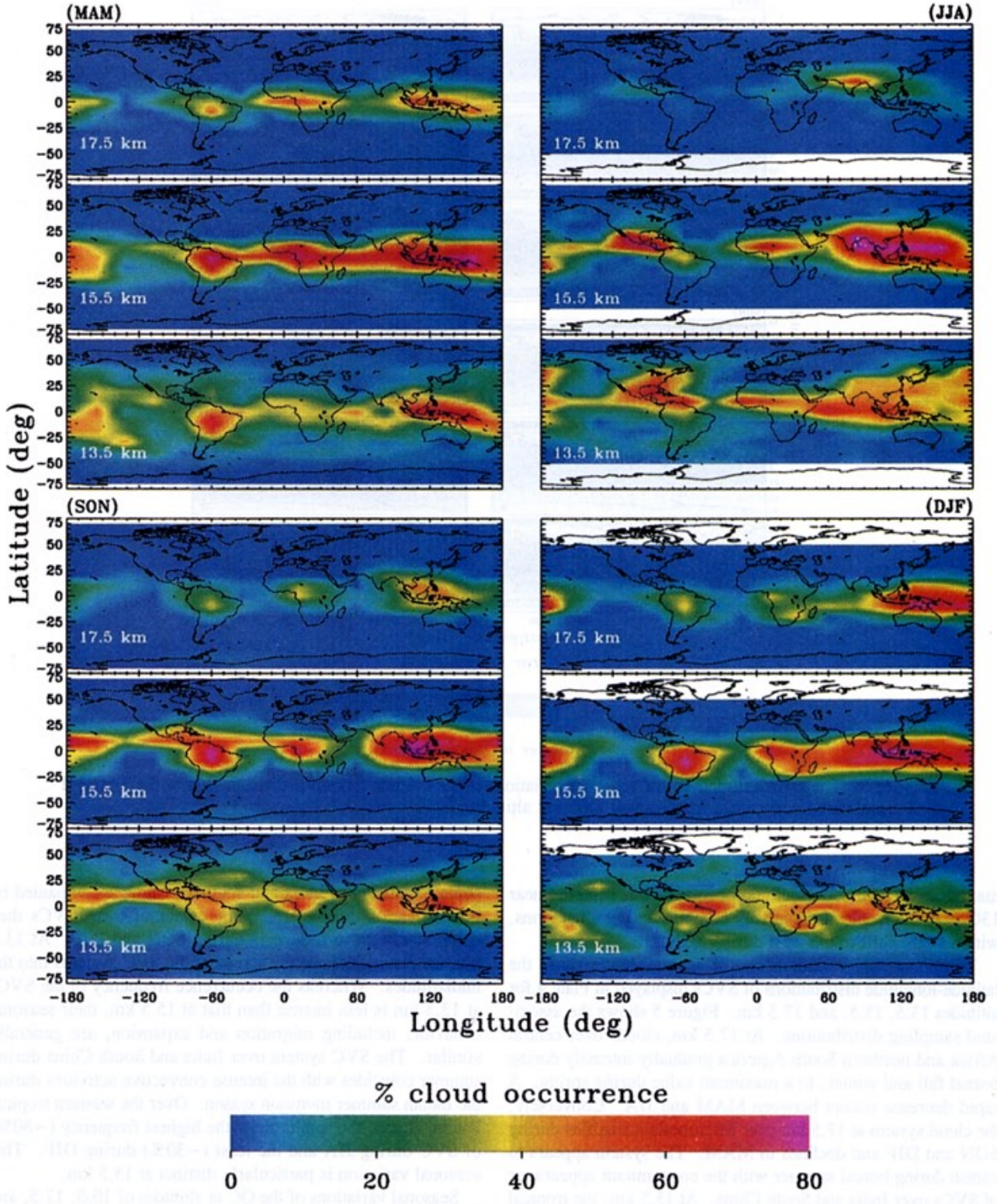

Plate 4. Seasonal variations of the latitude-longitude distributions of the SAGE II subvisual cloud occurrence frequency at different altitudes.

the troposphere expands vertically by about 1 km, the OC diminishes slightly. The OCs occur less frequently at all altitudes between 30°N and 70°N during the fall. The seasonal variability in the southern middle and high latitudes (70°S–30°S) mirrors the variations in the northern middle and high latitudes. The OCs occur more often during the austral spring and summer than other seasons. Although the winter disturbances due to long waves in the southern hemisphere are less intense than in the northern hemisphere, the enhanced longitudinal variations of the OC occurrence in winter are noticeable. Such a seasonal variation in the longitudinal distribution is also evident in the subvisual clouds. The

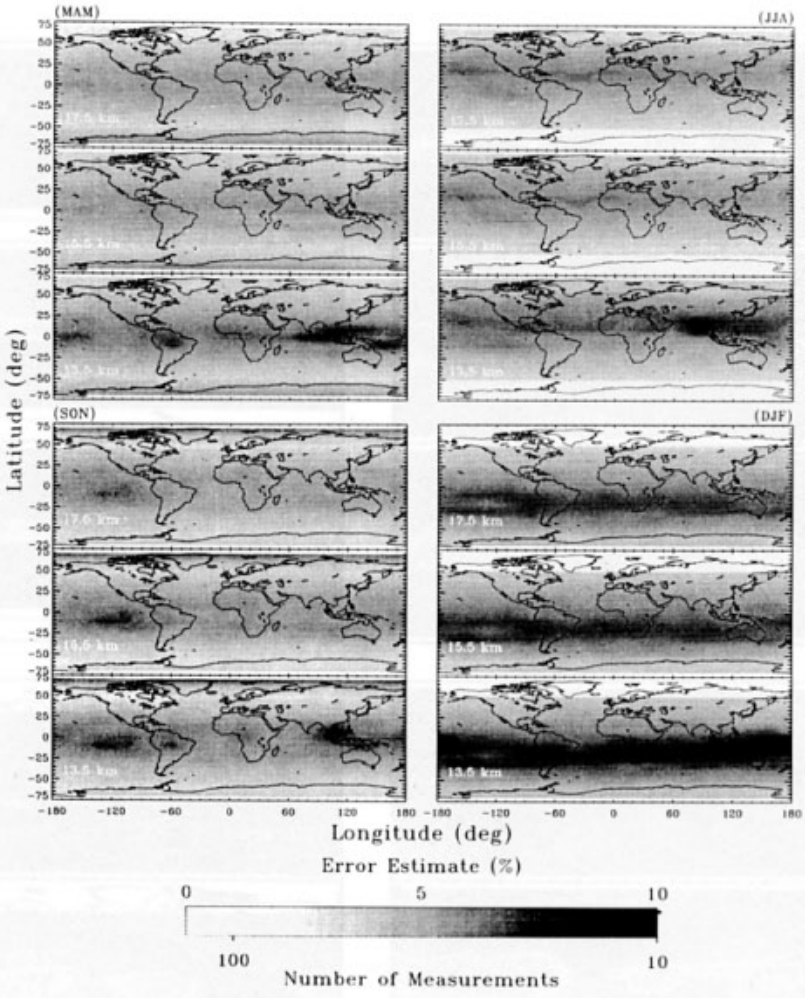

Figure 5. The error estimate of the seasonal variations of the latitude-longitude distributions of the SAGE II subvisual cloud occurrence frequency at different altitudes.

maximum in both subvisual and opaque clouds centered near 130°E in the tropics is relatively constant during all seasons, with a slight shift to the west during SON.

These seasonal variations can be seen more clearly in the latitude-longitude distributions of SVCs displayed in Plate 4 for altitudes 13.5, 15.5, and 17.5 km. Figure 5 shows the associated sampling distributions. At 17.5 km, clouds over central Africa and northern South America gradually intensify during boreal fall and winter, to a maximum value during spring. A rapid decrease occurs between MAM and JJA. Conversely, the cloud system at 17.5 km over Micronesia intensifies during SON and DJF and declines in MAM. The system appears to vanish during boreal summer with the concomitant appearance of SVCs over India and South China. At 15.5 km, the tropical SVC system over northern South America is relatively stable throughout the entire year, except during JJA when the SVC system shifts to Mexico. While declining during JJA, the SVCs over central Africa move northward by about 10°–15°. The SVCs reappear over central Africa during SON and move farther south as the cloud system intensifies during DJF. The SVCs then return to central Africa during MAM. As noted earlier, the SVCs over Micronesia (~120°E over the equator) at 15.5 km are generally stable throughout the year. There is some expansion to India and southern China accompanied by intensification during JJA. The center of these SVCs then shifts southeast to Indonesia during SON and DJF. At 13.5 km, the results indicate the spread of the SVC systems into the midlatitudes. Whereas the occurrence frequency of the SVCs at 13.5 km is less intense than that at 15.5 km, their seasonal behavior, including migration and expansion, are generally similar. The SVC system over India and South China during summer coincides with the intense convective activities during the Indian summer monsoon season. Over the western tropical Pacific Ocean, the results show the highest frequency (~80%) of SVC during JJA and the least (~30%) during DJF. This seasonal variation is particularly distinct at 13.5 km.

Seasonal variations of the OC at altitudes of 10.5, 12.5, and 14.5 km are displayed in Plate 5 with the corresponding sampling patterns in Figure 6. While the occurrence of OC is generally less frequent than that of the SVC, the OC and SVC seasonal behaviors are similar. This similarity is especially true for the seasonal variations of clouds associated with the Indian summer monsoon and the seasonal migration of the cloud systems over Africa and northern South America. The same seasonal features are also evident in the climatology of high-altitude clouds of *Warren et al.* [1986, maps 176–179],

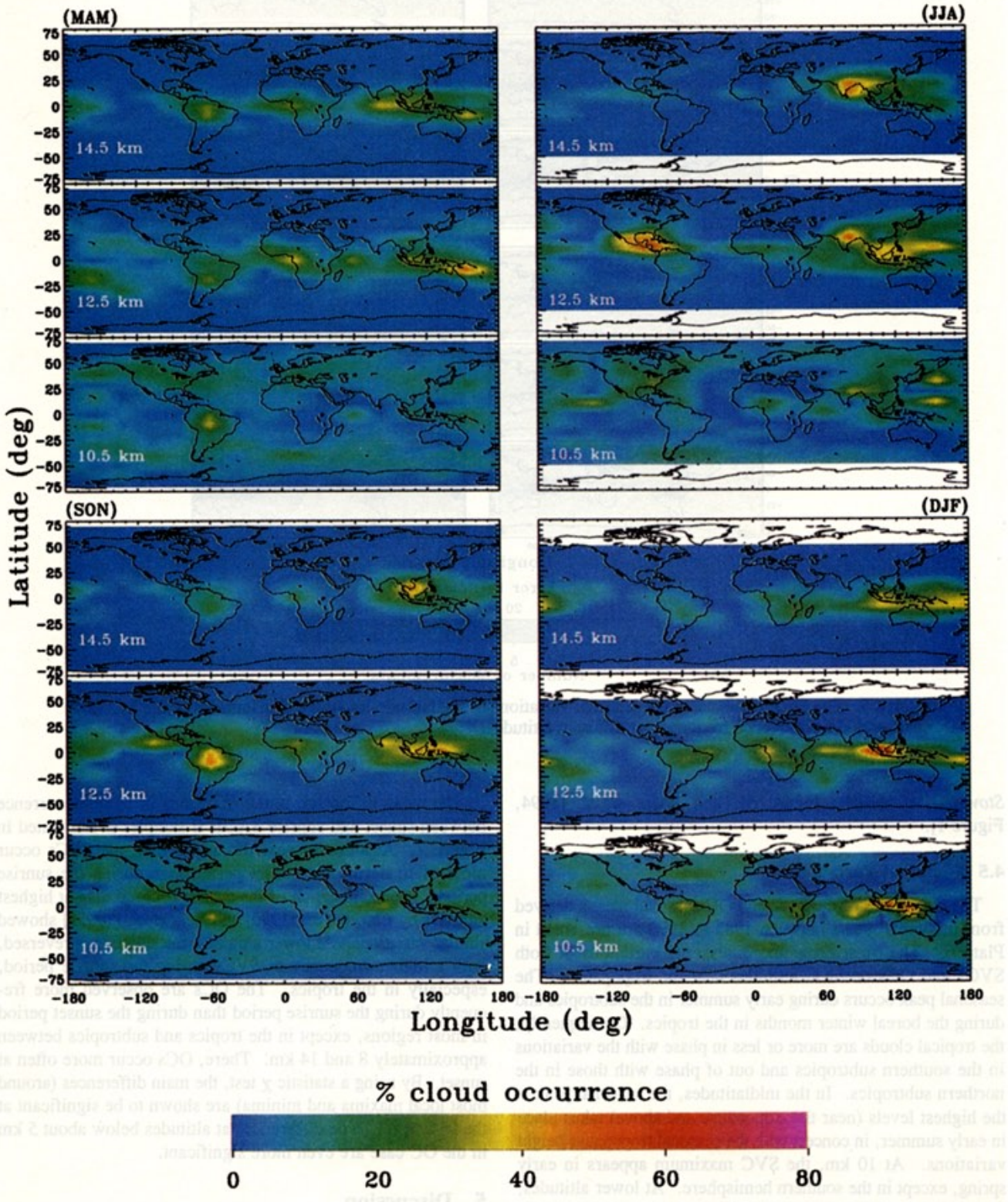

Plate 5. Seasonal variations of the latitude-longitude distributions of the SAGE II opaque cloud occurrence frequency at different altitudes.

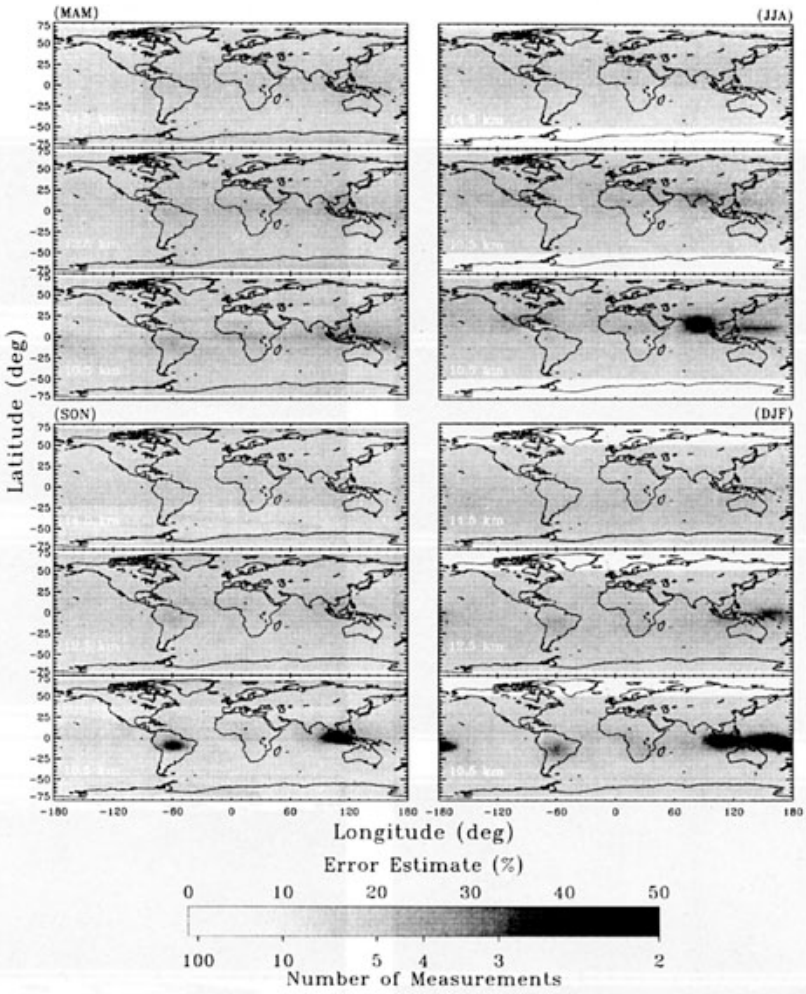

Figure 6. The error estimate of the seasonal variations of the latitude-longitude distributions of the SAGE II opaque cloud occurrence frequency at different altitudes.

Stowe et al. [1989, Figure 6], and *Wylie et al.* [1994, Figure 1].

4.5 Temporal Variations

The time series of the SVC and OC seasonal means derived from individual years between 1985 to 1990 are presented in Plate 6. The most pronounced seasonal variations of both SVCs and OCs occur at altitudes near the tropopause. The seasonal peak occurs during early summer in the subtropics and during the boreal winter months in the tropics. Consequently, the tropical clouds are more or less in phase with the variations in the southern subtropics and out of phase with those in the northern subtropics. In the midlatitudes, the seasonal peak at the highest levels (near the tropopause and above) takes place in early summer, in concert with the seasonal tropopause height variations. At 10 km, the SVC maximum appears in early spring, except in the southern hemisphere. At lower altitudes, seasonal changes in cloud frequency are less apparent, except in the lowest layers at northern midlatitudes. There, OCs occur more frequently during winter and spring than during summer and fall. Variations in the columnar integrated frequency were computed in order to explore possible trends in the data. The results show no apparent trends in the total cloud frequency from 1985 to 1990.

The mean difference in the frequency of cloud occurrence between sunset and sunrise SAGE II samples is illustrated in Figure 7. At altitudes near the tropopause, the SVCs occur more often during the sunset period than during the sunrise period. The examination of the SAGE II cloud data at highest altitudes by *Chiou et al.* [1990] and *Kent et al.* [1995a] showed similar variations. At lower altitudes, the situation is reversed, with a higher frequency of SVCs during the sunrise period, especially in the tropics. The OCs are observed more frequently during the sunrise period than during the sunset period in most regions, except in the tropics and subtropics between approximately 8 and 14 km. There, OCs occur more often at sunset. By using a statistic χ test, the main differences (around most local maxima and minima) are shown to be significant at the 95% level. The differences at altitudes below about 5 km in the OC case are even more significant.

5. Discussion

The SAGE II cloud analyses provide a unique perspective on the vertical structure of global cloudiness that complements other cloud climatologies. Surface observations typically report only those clouds that are unobscured by lower clouds. Most satellite analyses only sample the uppermost clouds, yielding a bias opposite that of the surface observer. It is

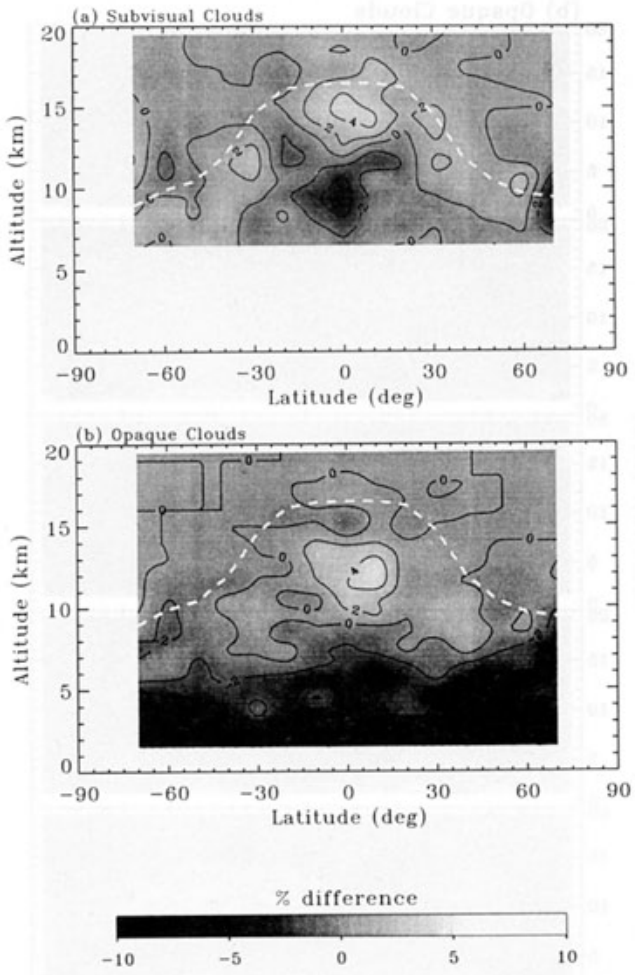

Figure 7. Difference in the cloud occurrence frequency between SAGE II sunrise and sunset observations (sunset minus sunrise) for (a) subvisual and (b) opaque clouds. The dashed lines indicate the tropopause.

difficult to determine from satellite imagery how deep a cloud extends into the atmosphere regardless of its optical depth. While SAGE II cannot directly provide values for cloud fractional coverage or determine the layering of clouds underneath optically thick ($\tau > 0.03$) clouds, it does indicate how often a cloud occurs in a given layer for all levels unobscured by higher clouds. Thus these SAGE II analyses provide new information about the vertical structure of subvisual cirrus clouds and reveal, for the first time, the seasonal and geographic variability of high-altitude subvisual clouds and their relationship to opaque cloudiness.

5.1 Uncertainties in Occurrence Frequencies

Uncertainties in the derived cloud frequency arise from three major factors, including the sampling rate and distribution dictated by the solar occultation technique and the sampling volume imposed by the instrument. The sampling rate determines directly the total population of the measurement in space and time, while the sampling distribution governs essentially the capability of the observation for resolving fine structures in space and time. The sampling volume determines the spatial coverage of the measurements.

The error in the derived cloud frequency over a given region during a specific period is inversely proportional to the number of observations. As examples, Figures 5 and 6 show the uncertainties associated with the data population used in the cloud frequency analysis displayed in Plates 4 and 5, respectively. In general, the uncertainty in the cloud frequency decreases as altitude increases, consistent with the reduced sampling size at lower altitudes due to the presence of opaque clouds in high altitudes. At lower altitudes, the error distributions resemble the patterns of the OCs. Because Figures 5 and 6 are the distributions of the total measurement population, they can be applied to both SVCs and OCs.

Regarding the error associated with the constraint in sampling distribution, as indicated in section 2, the solar occultation technique repeats its measurements at a given latitude with a frequency of about a month. Thus the SAGE II observations do not contain information concerning changes in cloud distributions with shorter frequencies. For this reason, the derived seasonal cloud frequency could be biased. Quantifying this type of bias is very difficult. Clearly, the bias is unlikely to be determined based on SAGE II observations alone. To provide an estimate, one must use data with higher sampling frequency from different observational systems. In the present analysis, the cloud-frequency bias is examined based on the standard deviations in the total cloud amount compiled by *Warren et al.* [1986, 1988]. In the tropics, the bias estimate for a grid of 10° X 24° with two sampling points per season is about 8% over 6 years (six individual seasons). At midlatitudes (40°–50°), where the SAGE II sampling opportunity is about 1 order of magnitude better [*McCormick,* 1987], the estimate shows a typical seasonal bias over the ocean between 2% and 3% in the northern hemisphere and about 3% in the southern hemisphere. The estimate at northern midlatitudes over land is between 3% and 4%. These potential regional biases will be significantly reduced if averaged over large areas.

The uncertainty related to the constraint in sampling volume of the satellite instrument is perhaps more severe than that associated with the sampling rate and distribution, particularly because of the constraint of a 200-km sampling length (section 2). In the present paper, the SVCs have been defined as those with optical depths less than approximately 0.02–0.03 (Figure 1). This standard definition [e.g., *Sassen and Cho,* 1992], when applied to the SAGE II data, requires some critical assumptions. The SAGE II extinction saturation limit of about 0.02 km^{-1} is based on the assumption that the observed cloud extends over the entire 200-km path length of a 1-km-thick layer. In such cases, the optical depth of the cloud in the vertical direction might be some value greater than 0.02, depending on the actual total length of the cloud elements in the SAGE II 200-km path length. The exact optical depth limit τ_{max} for a given case is roughly equal to 0.02 X 200 (km) ÷ C where C is the total length of the cloud elements in the SAGE II path length. For example, if C = 1 km, τ_{max} = 4. Thus the possible range in optical depths for these subvisual clouds is approximately 0.02–4. As a result, it is probable that some fraction of the subvisual cloud occurrences corresponds to visibly detectable cirrus clouds. The mean extinction coefficient for the subvisual clouds in the SAGE II data set is about 0.008 km^{-1} [*Wang et al.,* 1995a], which corresponds to a mean optical depth range of 1.6–0.008 for cloud length *(C)* varying from 1 to 200 km, respectively.

Liao et al. [1995a] also performed an analysis of SAGE II clouds for comparison with the ISCCP high cloud amounts.

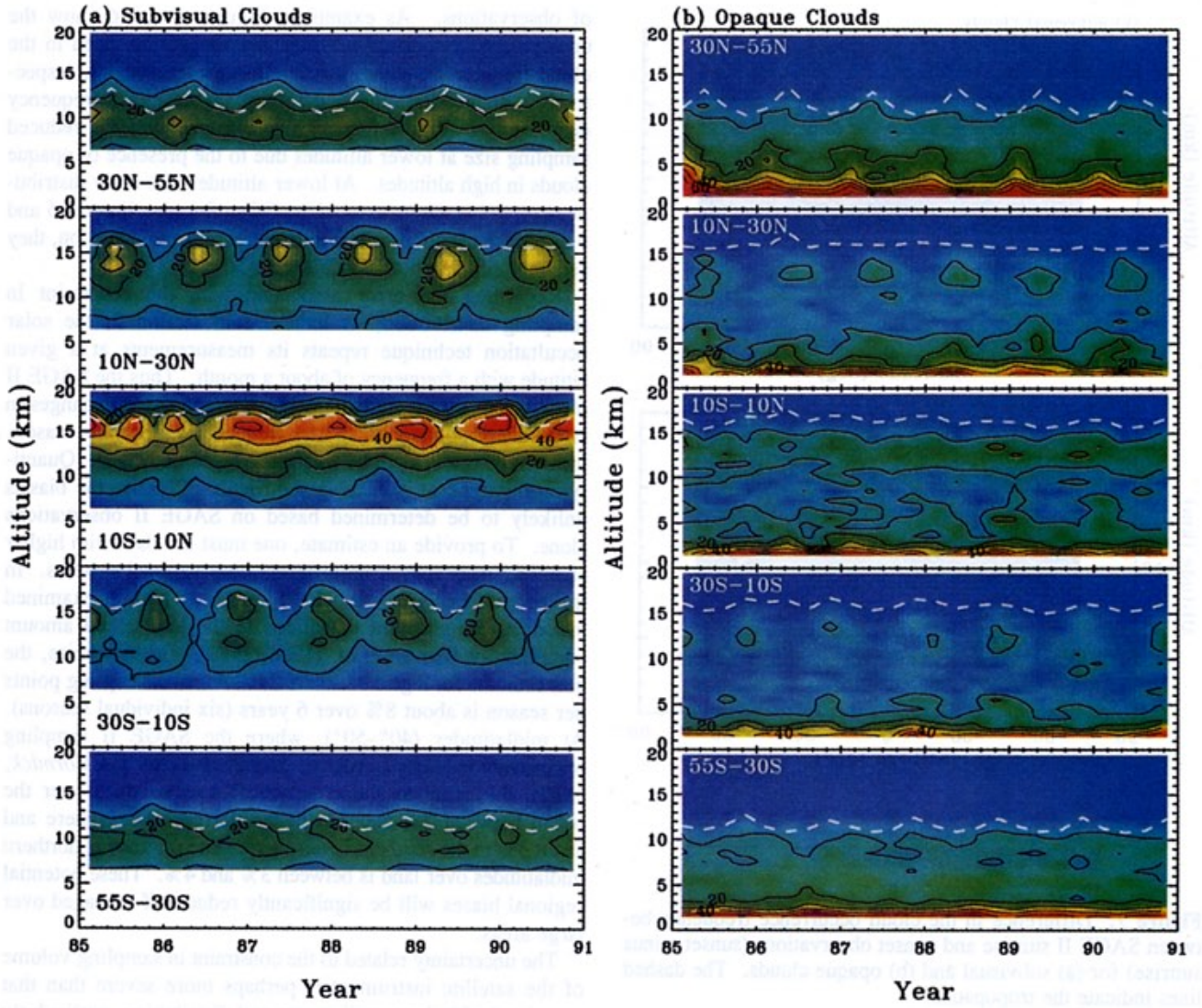

Plate 6. Time series of the (a) subvisual and (b) opaque cloud occurrence frequency in the tropics and at mid-latitudes. The dashed lines indicate the tropopause. The color scale is the same as in Figure 2.

The ISCCP analysis technique can detect clouds with optical depths as low as 0.1 under certain conditions. Using definitions for cloud occurrence, extinction, and amount different from the present analysis, *Liao et al.* [1995a] deduced that ISCCP and SAGE II high cloud amounts could be matched if it is assumed that only values of the extinction coefficient *(k)* greater than about 0.008 km^{-1} correspond to clouds and C = 75 km for Δz = 2.5 km. It has not been shown conclusively that the true mean value of C is 75 km, especially with regard to the SVCs. However, it appears to be a reasonable value considering that it converts to a cloud amount of 37.5% and that the average cirrus amount-when-present from surface observations [*Warren et al.*, 1986, 1988] is 38.1%. Using C = 75 km and k = 0.008 km^{-1} yields τ = 0.021 for Δz = 1 km, a value within the standard SVC definition. From *Wang et al.* [1995a], it is clear that almost 70% of the unsaturated extinction coefficients are less than 0.008 km^{-1}. The mean extinction coefficient for the SVCs in the SAGE II data set is also 0.008 km^{-1}, indicating that the mean optical depth for the SVCs corresponds to the *Sassen and Cho* [1992] definition. If the SVCs are limited to those clouds having $\tau < 0.03$ and C = 75 km, then based on the results of *Wang et al.* [1995a], approximately 80% of the observed SVCs truly correspond to the actual SVCs. The remaining 20% would be marginally subvisual and may still be difficult to detect from the surface and more conventional satellite analyses.

The SVC definition also assumes that the cloud extends over the entire 1-km layer corresponding to the SAGE II measurement. The exact vertical extent of the observed cloud is unknown due to the resolution of the measurements. Therefore the actual optical depth relative to the vertical is likely to be less than the reported value, further increasing the probability that a given SVC has $\tau < 0.03$. The cloud frequencies in each layer are reported independently of other layers. Thus, if a particular cloud occupies more than one contiguous layer, it will be reported for each layer in which it occurs. Summing the optical depths for the contiguous layers may increase the total optical depth beyond the threshold for subvisual clouds. This effect may not be particularly important since the physical thickness of the SVCs can exceed 4 km [*Sassen and Cho,*

1992]. Given these caveats and assuming that the *Liao et al.* [1995a] value is reasonable, it is concluded that most of the SVCs observed by the SAGE II instrument fit the standard definition of the SVCs and are unlikely to be observed by surface observers or most meteorological satellite sensors.

All of the OC occurrences fit the given definition. The actual number of occurrences may be slightly biased based on the earlier discussion concerning the true cloud path length and the SVCs. Any overestimate of the SVCs is balanced by a corresponding underestimate of the OCs. As noted earlier, the frequency of occurrence of the OC will be overestimated at lower levels over regions containing land features above 1 km. The overestimation will depend on the fraction of the region containing land at a given level.

5.2 SVCs and OCS

As shown in Figures 2–6 and Plates 1–6, there is close correspondence between the SVC and the upper-level OC in terms of temporal and spatial patterns of cloudiness. The spatial patterns in the SVC (Plate 1a) are also very similar to the transmissive cloud probabilities derived by *Wylie et al.* [1994] using HIRS data. The apparent strong coupling suggests that most subvisual cloudiness might be derived from active storm centers and deep convection or from their cirrus outflow. The convective mechanism is the most obvious for forming high-altitude clouds between 15 and 20 km in the tropics. Following the onset of convection, sufficient water vapor should be available for forming cloud particles, especially at such low temperatures near the tropopause as the lifted air spreads in the upper layers. The light winds at those altitudes in the tropics will slowly mix the moist air with the drier air, possibly producing relatively long lived clouds. Probably most clouds that reach the highest altitudes (> 15 km) are from the active centers of the deepest convective clouds [e.g., *Danielsen*, 1982a, b, 1993]. Thus there is a maximum in tropical SVCs around 15.5 km that diminishes by a factor of 2 or more at 18.5 km.

The maximum OC occurs between 12 and 15 km, for example, Figure 2. *Zhang* [1993] found that the fractional coverage by deep convective clouds in the tropics decreases by a factor of 2 or more as cloud top altitude increases from 15 km to higher altitudes. There may be fewer SVCs observed at 12.5 km than at 14.5 km because the greater occurrence of OCs at those altitudes diminishes the opportunities for the SVC either to form or to be observed. The optically thick high clouds observed by *Zhang* [1993] over the tropics (20°S–20°N) displayed a distinctive seasonal pattern that peaked during January. A similar seasonal pattern is not well defined in the OC variations in Plate 6. However, the SVCs between 10°S and 10°N undergo a seasonal cycle with peak values around January, providing additional confirmation of the correspondence between deep convection and SVC occurrence. This correspondence is also evident at the diurnal scale. In Figure 7, the evening maxima in high-altitude SVCs coincide with the evening peaks in OCS at slightly lower levels.

At the highest levels in the tropics, the SVCs are confined primarily to the convective centers with little horizontal spreading (Plate 1a). These high levels (> 18 km) may be located above the local tropopause, resulting in a rapid dissipation of the clouds in the drier stratospheric air. Between 14 and 18 km, there is a relatively sharp frequency gradient in the SVC contours between the tropics and midlatitudes, presumably conforming to the tropopause heights (Plate 1a). Some SVCs persist in the subtropics at altitudes between 10 and 14 km, although they diminish significantly below 12 km.

In many instances, especially in the midlatitudes, frequent occurrences of SVCs are evident above the mean tropopause (e.g., Figure 2). Because the tropopause can vary by several kilometers about the mean zonal value, it cannot be concluded that all of the SVCs above the mean tropopause altitude were in the stratosphere. Most of the midlatitude SVCs probably occur within the troposphere and are associated with disturbances along frontal boundaries. In cyclonic systems, cirrus clouds occur in the upper levels of warm sector air masses having tropopause heights that are generally greater than the mean. Thus, if midlatitude SVCs are the precursors of visible cirrus in warm fronts, then they probably originate in the upper reaches of the warm sector of the troposphere. They may enter the stratosphere as part of the occluded air masses or through tropopause folding events.

That scenario is consistent with the variations in the mean SVC relative maxima north of 20°N. The maxima occur to the east of the annual average positions of the two most distinctive 200-hPa troughs centered along the east coast of the United States and Asia [*Oort*, 1983]. The axes of these maxima follow the mean 200-hPa heights eastward to the ridges. For example, in Plate 1a at 10.5 km, an SVC maximum extends from approximately 33°N, 160°E to 40°N, 120°W. Similarly, another relative SVC maximum extends from about 30°N, 70°W to 50°N, 0° longitude. The one prominent midlatitude relative maximum at 12.5 km in the northern hemisphere also occurs northeast of the mean trough position near the east coast of the United States. West of the mean ridge locations over the United States and Asian west coasts, the SVCs are relatively infrequent. A mean trough-and-ridge structure is not well defined over Europe and Asia, consistent with the diffuse nature of the SVC maxima over Europe and most of Asia. Although the mean annual 200-hPa heights are almost zonal in the southern hemisphere [*Oort*, 1983], there is a minor ridge/trough along the west/east coast of South America. The relative maxima west/east of the ridge/trough are similar to those around the United States.

It is likely that SVCs are not all directly formed as part of the same systems generating OCs. As shown in Figures 2–6 and Plates 1–6, the frequency of SVCs is about 2 to 3 times that of the high-altitude OCs, while they are formed over more or less the same general geographic areas. The differences in the horizontal coverage (Plate 1) and the lifetimes of the these two types of clouds may account for much of the observed frequency differences. However, some of the SVCs may form in situ due to slight lifting of marginally saturated air [*Heymsfield*, 1993]. Further investigations are needed for a definitive conclusion regarding the mechanism(s) controlling the in situ formation of SVCs. Nevertheless, the correspondence of the SVC to times and locations favorable to the cirrus formation is not surprising. It provides evidence that SVCs are related either directly or indirectly to the development of ordinary cirrus clouds or cumulonimbus anvils.

5.3 Diurnal Variations

The diurnal changes in the OC clouds are consistent with other satellite-derived cloud data . For example, *Minns and*

Harrison [1984] found an 1800 LT (local time) maximum in high clouds over land area where deep convection predominated. The diurnal phase varied for high clouds over other land areas. Although high cloud maxima occurred at a different time of day over ocean areas, most of marine high cloudiness peaked during the afternoon and evening according to the Minnis and Harrison studies. Thus the pronounced evening OC maximum near 13 km in the tropics is probably dominated by the deep convection arising from solar heating of the land surfaces of the Amazon Basin, central Africa, and the maritime continent. The minimal evening high-altitude OC maxima in the subtropics and midlatitudes are probably dominated either by the weak ocean afternoon peaks or by spring-summer deep convection over the land areas.

The evening maxima in the high-altitude SVCs probably result from the same processes driving the OC diurnal variations. The relative minimum over the tropics at 9 km is probably due to obscuration by or the presence of the OC clouds at or above 9 km during the afternoon. Overall, the magnitudes of the SVC variations are slightly greater than or equal to the OC diurnal changes. Relative to their overall frequency, however, the OC diurnal ranges at a given altitude are larger than the corresponding SVC diurnal changes. The morning maxima in the OC below 5 km are probably due to the strong diurnal cycles in marine stratocumulus and in stratus and altostratus over many land areas [e.g., *Minnis and Harrison*, 1984].

5.4 Radiative Effects of SVCs

Subvisual cloudiness is generally not a consideration in most climate simulations or calculations of radiative transfer in the atmosphere. The average optical depth at visible wavelengths is small. However, the frequent occurrence of SVCs, particularly in the tropics, calls for an assessment of the potential impact of SVCs on the radiation budget. To estimate these effects, it is assumed that the SVC particles are ice spheres with a mean effective radius of 1 μm and an effective variance of 1 [*Heymsfield*, 1993; *Wang et al.*, 1995a]. Mie scattering calculations yield an extinction efficiency of 2.28 at a wavelength (λ) of 0.65 μm. The extinction efficiency is 0.335 at $\lambda = 10.8$ μm. These wavelengths were selected because they are used for remote sensing and are close to average value for the broadband shortwave (0.2–5.0 μm) and longwave (5–50 μm) spectra [e.g., *Minnis et al.*, 1993]. The mean visible optical depth of 0.021, estimated for the SVC, converts to 0.0031 for $\lambda = 10.8$ μm.

The greatest longwave effects from SVCs should occur in the tropics for cold clouds over the hottest backgrounds. A typical clear-sky longwave flux over the tropical oceans is 295 W m^{-2}. Assuming a cloud temperature of 200 K, the cloud emitted irradiance is 91 W m^{-2}. Using a diffusivity factor of 1.66 yields an effective longwave optical depth of 0.0052. A simple radiative transfer calculation produces a longwave flux at the top of the atmosphere of 293.9 W m^{-2} for the clear scene with the mean SVC overhead. Thus, on average, when a subvisual cloud is present in otherwise clear skies, the outgoing longwave flux will be reduced by -1 W m^{-2}. This decrease diminishes for small contrasts between the SVC and the background temperatures. A 10.8-μm radiance for a clear scene with an effective blackbody temperature of 295 K would be reduced by only 0.1–0.2 K for viewing zenith angles between 0° and 45°.

The SVC effects on shortwave albedo were computed with the method of *Fu and Liou* [1994] over a tropical ocean background to maximize the impact. For clear skies, the albedos are 0.0870, 0.1008, and 0.1331 at solar zenith angles 0°, 45°, and 70°, respectively. The mean SVC increases the respective albedos by only 0.0002, 0.0005, and 0.0023. These results indicate a minimal impact on albedo that is beyond the level of detection for most nadir-viewing passive instruments. At a solar zenith angle of 45°, the mean SVC increases the albedo by 0.5% for the dark clear ocean. Over any other surface such as land or clouds, the net change will be smaller. If the maximum impact is considered on a 24-hour basis, the average SVC will increase the reflected solar energy by -0.5 W m^{-2}. Because of the greater longwave effect, the mean maximum change in the top-of-the-atmosphere net flux is $+0.5$ W m^{-2} for a 1-km-thick cloud. Thicker SVCs will produce greater warming. This value will be smaller, however, for SVCs over other backgrounds and for nonovercast SVC conditions. In summary, these estimates indicate that the SVCs can produce a net warming of the Earth-atmosphere system that is similar in magnitude, but opposite in sign, to the direct forcing estimated for anthropogenic tropospheric aerosols [*McCormick et al.*, 1995].

5.5 Stratosphere-Troposphere Exchange and Dehydration

The formation of high-altitude clouds has a very important implication for the stratosphere troposphere exchange (STE) and dehydration processes [e.g., *Russell et al.*, 1993; *Holton et al.*, 1995]. It is well established that the dry stratosphere is maintained by the passage of tropospheric air through the cold tropopause [e.g., *Newell and Gould-Stewart*, 1981; *Mote et al.*, 1996]. Also, the zonal-temporal averaging yields an upward transport of tropospheric air into the tropical stratosphere and a compensating downward transport of stratospheric air into the troposphere at extratropical latitudes. The thermal effect of this eddy-driven mean zonal circulation is to maintain the temperature in the extratropical atmosphere above radiative equilibrium and to keep the temperature in the tropics below radiative equilibrium [e.g., *Holton*, 1990]. The zonally averaged tropical tropopause temperatures are not cold enough to dehydrate air to the observed lower stratospheric water vapor mixing ratio. Therefore the tropospheric air that could enter the stratosphere in the tropics must be confined to areas where the tropopause temperature is close to the frost point necessary to remove moisture. By analyzing available temperature data at 100 mbar in the tropics, *Newell and Gould-Stewart* [1981] identified the western tropical Pacific Ocean, northern Australia, Micronesia, and the Bay of Bengal and India as the appropriate regions where air enters the stratosphere. The months from November to March are the favorable period for the STE processes to take place over the western tropical Pacific Ocean, northern Australia, and Micronesia, while the summer monsoon is the favorable time over the Bay of Bengal and India.

Because the formation of clouds and precipitation is essential for removing moisture, regions favorable for the cold trap dehydration mechanism must coincide with locations having intensive cloud activities. Indeed, the places and times having

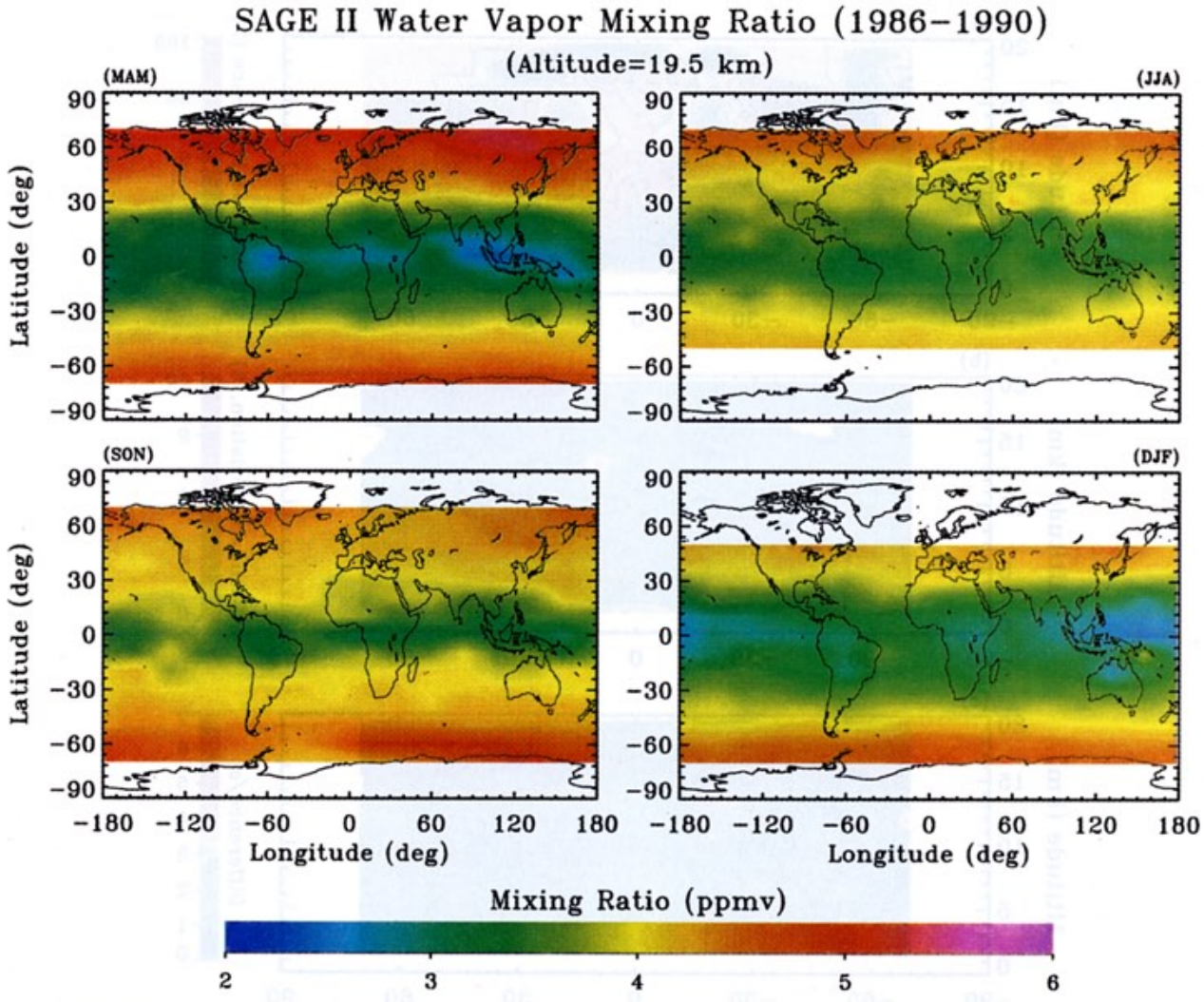

Plate 7. Seasonal water vapor distributions at an altitude of 19.5 km derived from SAGE II observations from 1986 to 1990.

the coldest temperatures [*Newell and Gould-Stewart,* 1981] are consistent with the areas and seasons of frequent high-altitude clouds of the 6-year SAGE II cloud climatology (Plates 1, 4, and 5). To further substantiate the connection of the STE, dehydration, and high-altitude clouds, the seasonal water vapor distributions at an altitude of 19.5 km are derived from the SAGE II observations, as shown in Plate 7. Readers are referred to *Chu et al.* [1993] for a detailed description of the SAGE II water vapor measurements. The altitude of 19.5 km was chosen for the illustration because it is in the stratosphere and close to the tropical tropopause. This choice is made also for minimizing the effect of clouds on the water vapor distribution analysis, which is known for interfering with the SAGE II water vapor measurements [*Chu et al.,* 1993]. As anticipated, the regions with lowest water vapor concentration (<3 parts per million by volume (ppmv)) are located close to maxima in high-altitude clouds. The timing of the STE processes also roughly corresponds to the high-altitude cloud variations (Plate 4).

During January–February 1987, an intensive field experiment was conducted to investigate the STE and dehydration processes in the western tropical Pacific Ocean and northern Australia under the Stratosphere-Troposphere Exchange Project (STEP Tropical) [*Russell et al.,* 1993]. The STEP Tropical results show the first in situ evidence of the convective scale cold trap that dries air of tropospheric origin to the prevailing stratospheric lowest water vapor mixing ratio (<3 ppmv). It is not surprising then that the winter SAGE II water vapor measurements over the western tropical Pacific Ocean and northern Australia show lowest seasonal mixing ratios (<3 ppmv) (Plate 7), while the 6-year cloud climatology indicates highest seasonal cloud (SVC) frequencies over the same geographic areas during the same period (e.g., Plate 4). This strong negative correlation between cloud occurrence and lower stratospheric water vapor mixing ratio and its timing over the western tropical Pacific Ocean and northern Australia provide satellite observational evidence on the delicate connection between the high-altitude cloud occurrence and the STE and dehydration processes important to the dryness of the stratosphere.

One of the most significant STEP Tropical achievements is on the precise dehydration mechanism that proceeds in the atmosphere [*Russell et al.,* 1993]. The STEP Tropical results indicate that the dehydration mechanism operates not only in the anvils of continental-maritime clouds but also in the anvils

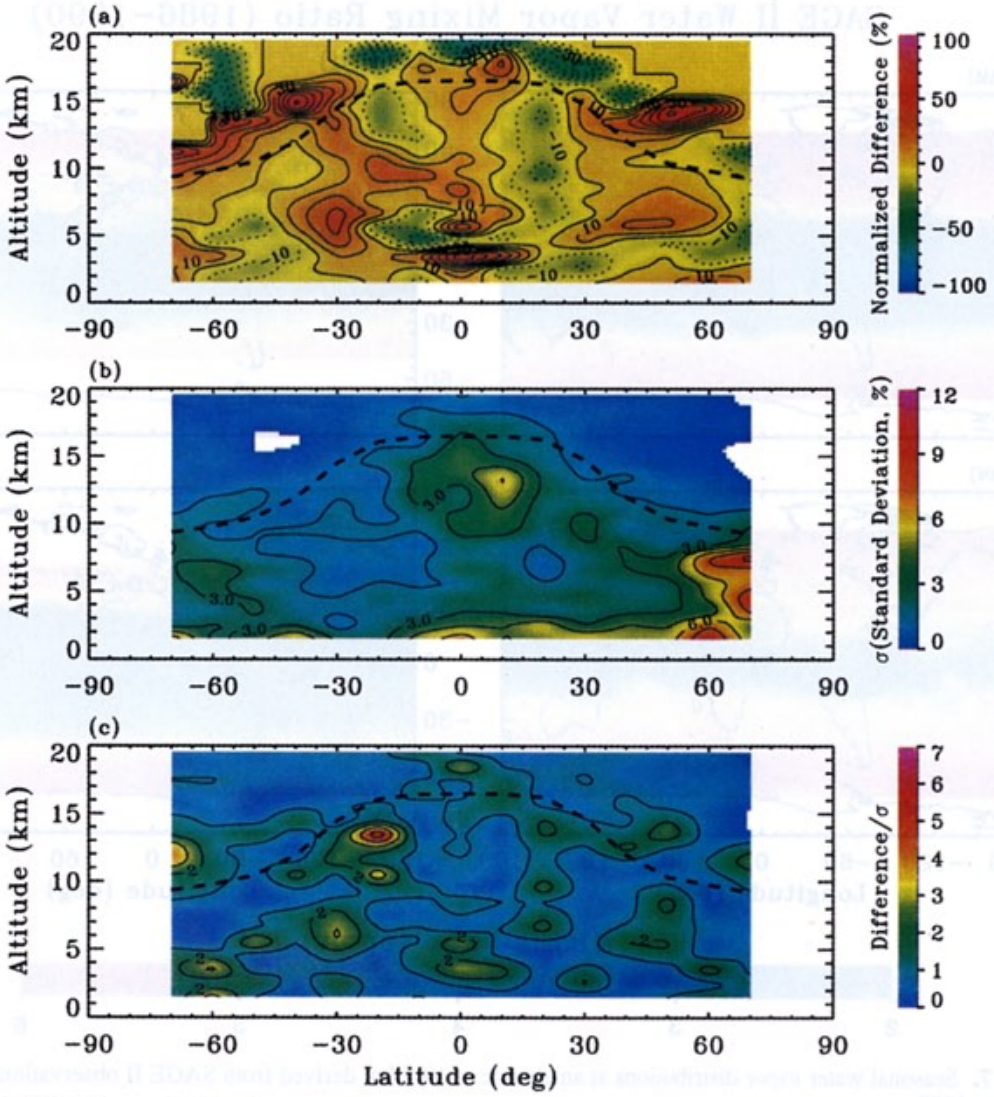

Plate 8. (a) Difference in cloud occurrence frequency between the 1987 ENSO period and the mean frequency from the five non-ENSO years (normalized to the mean) (b) Standard deviation of the cloud frequency derived from the five individual non-ENSO years (c) Ratio of the absolute frequency difference between the 1987 ENSO period and the mean frequency from the five non-ENSO years to the standard deviation of the five individual non-ENSO years.

of tropical cyclones and monsoon mesoscale (maritime) convective systems [*Danielsen,* 1993; *Russell et al.,* 1993]. The continental-maritime clouds are featured by deep turret overshooting and subsequent mixing in the lower stratosphere, indicating the operation of the dehydration-engine mechanism suggested by *Danielsen* [1982a]. The tropical cyclone clouds, on the other hand, involve a smooth large-scale lifting of the tropopause and the lower stratosphere with the formation of a large-scale cirrus shield. The development of the distinct large-scale cirrus cloud shield appears to follow closely the dehydration mechanism of the stratospheric fountain proposed by *Newell and Gould-Steward* [1981]; see also *Danielsen* [1993]. Although their dehydration potential is weaker than the continental-maritime and tropical cyclone clouds, maritime convective clouds exhibit greater potential for mixing air of tropospheric origin into the lower stratosphere due to the associated internal gravity waves [*Danielsen,* 1993]. Finally, the STEP Tropical observations also indicate rapid evaporation of small ice crystals that had been lofted into the warm lower stratosphere and resulting hydration of the local stratosphere [*Kley et al.,* 1982; *Knollenberg et al.,* 1993; *Russell et al.,* 1993]. Judging from the SAGE II cloud and water vapor observations in the tropics (Plates 4 and 7, respectively), the STE must be associated predominantly with dehydration, not with hydration.

5.6 ENSO, 1987

The SAGE II observations have been examined for the effect of the ENSO on tropical cloud occurrences at altitudes of 13.5–15.5 km by *Kent et al.* [1995a]. Their investigation indicates higher tropical cloud occurrence during the ENSO period than in the normal years. In the present investigation, the variations in cloud occurrence associated with the 1987

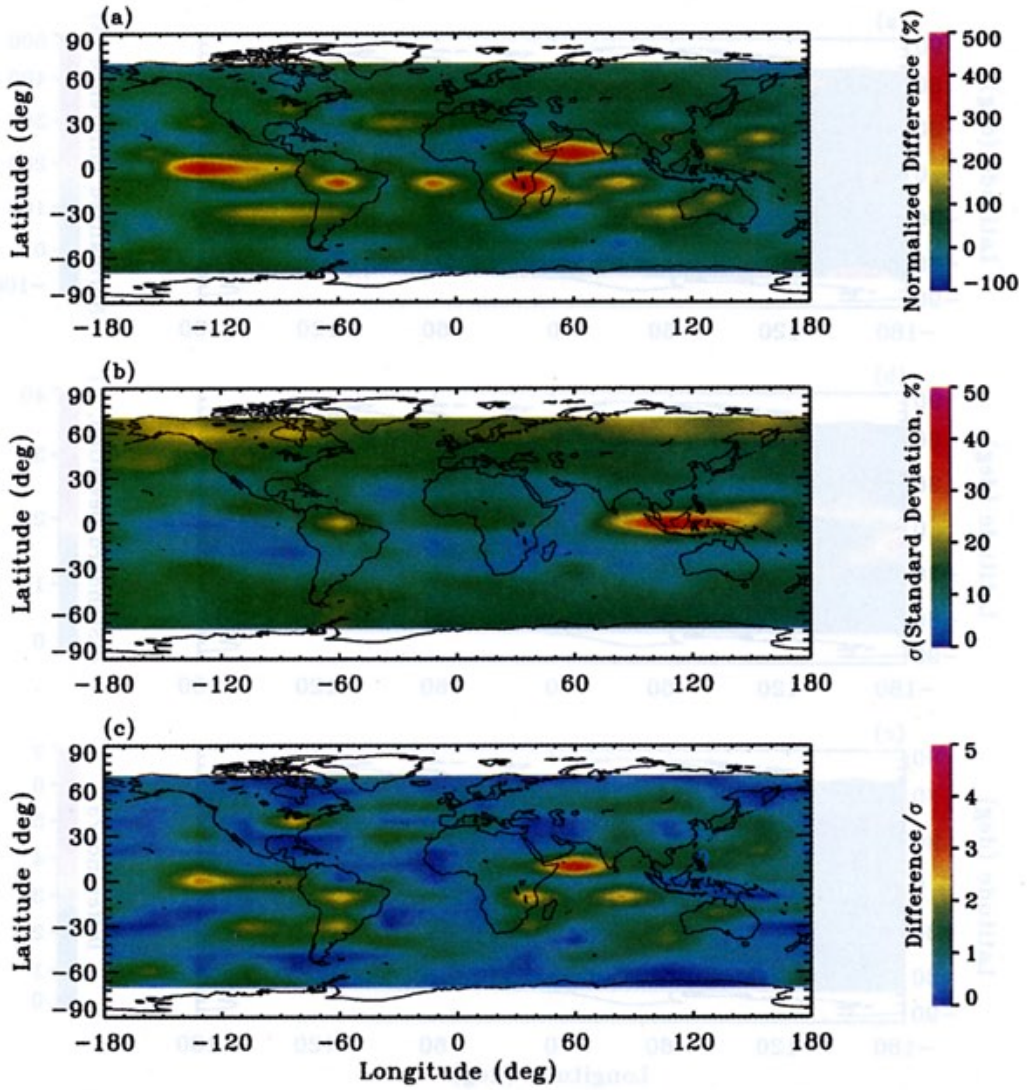

Plate 9. (a) Difference in cloud occurrence frequency between the 1987 ENSO period and the mean frequency from the five non-ENSO years (normalized to the mean) at an altitude of 7.5 km (b) Standard deviation of the cloud frequency derived from the five individual non-ENSO years at an altitude of 7.5 km (c) Ratio of the absolute frequency difference between the 1987 ENSO period and the mean frequency from the five non-ENSO years to the standard deviation of the five individual non-ENSO years.

ENSO event are examined with a global perspective. The zonal distributions of the differences in the total cloud frequency (sum of subvisual and opaque cases) between 1987 (an ENSO year) and the mean of the non-ENSO years (1985, 1986, 1988, 1989, and 1990) normalized to the mean of the non-ENSO years are drawn in Plate 8a. (This grouping of the SAGE II measurements is based on information of the sea surface temperature anomaly shown in Figure T4 of the *National Oceanic and Atmospheric Administration* [1995].) Several prominent features in the differences are clearly evident. The enhanced cloud occurrence in the tropics during 1987 is accompanied generally by reductions in cloud frequency in the subtropics, except at altitudes from 8 to 11 km in the southern hemisphere. The enhancement in a tropical layer centered at 3.5 km above the equator is particularly outstanding. A thin layer (1 km thick) of decreasing cloud frequency located at 4.5 km in the tropics is also apparent. Significant enhancements in cloud occurrence also take place between 30°N and 60°N during 1987, except in the layer at altitudes between 3 and 5 km. This layer of decreasing frequency extends beyond 60°N up to the tropopause. Additional regions of enhanced cloud occurrence are located between about 20°S and 40°S. Cloud frequency decreased between 40°S and 60°S during the 1987 ENSO year. The latitudinally alternating structure of the enhancement and reduction in cloud frequency follows the pattern of the large-scale tropospheric circulation to some extent, implying generally an intensified tropospheric circulation in the 1987 ENSO year. It has been suggested that the abnormal global precipitation distributions during ENSO years are the consequence of altered atmospheric circulation associated with ENSO events [*Lau and Sheu,* 1991]. Thus the concurrent reductions in cloud occurrence in the extratropical regions during an ENSO event are not surprising. Overall, there is an increase in tropospheric cloud occurrence, especially

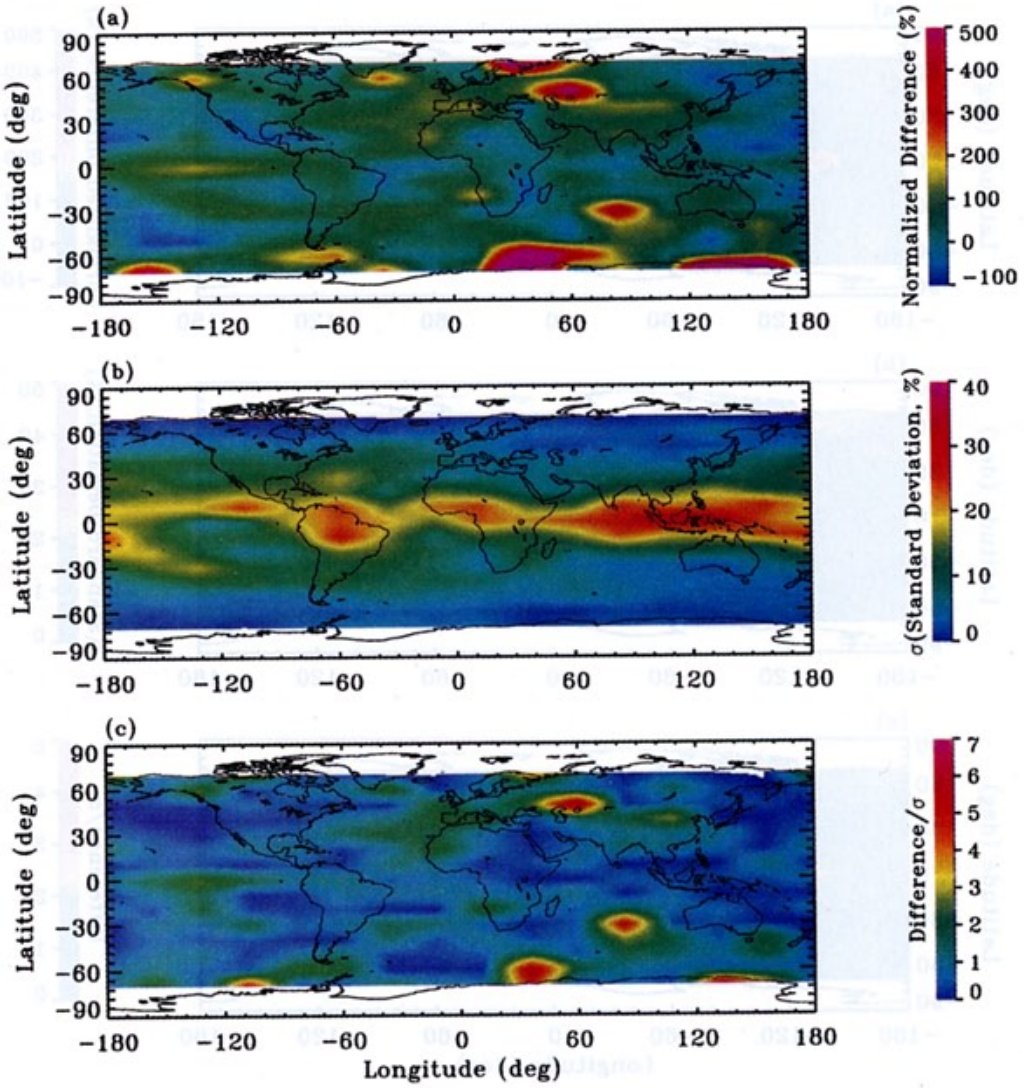

Plate 10. (a) Difference in cloud occurrence frequency between the 1987 ENSO period and the mean frequency from the five non-ENSO years (normalized to the mean) at an altitude of 12.5 km (b) Standard deviation of the cloud frequency derived from the five individual non-ENSO years at an altitude of 12.5 km (c) Ratio of the absolute frequency difference between the 1987 ENSO period and the mean frequency from the five non-ENSO years to the standard deviation of the five individual non-ENSO years.

in the tropics during the ENSO years. These results are similar to *Wylie et al.* [1994], who showed a significant increase in global high cloudiness during the 1991–1992 ENSO.

In order to examine the physical significance of the frequency differences between the 1987 ENSO year and the mean of the five non-ENSO years, the standard deviations of the cloud occurrence frequency are computed from the five individual non-ENSO years, as shown in Plate 8b. In general, high values of the standard deviation are shown at altitudes below about 4 km, at high latitudes about 50°, and at altitudes between approximately 9 and 16 km in the tropics. To examine the significance in the cloud frequency difference between the 1987 ENSO event and the non-ENSO period, the frequency difference is compared with the standard deviation of the five non-ENSO years. Plate 8c displays the ratio of the magnitude of the frequency difference to the standard deviation. The results indicate that the frequency differences in the subtropics and northern midlatitudes are significant at the 95% level. The frequency differences are highly significant at the low and middle altitudes south of 10°N.

The latitude-longitude distribution of the normalized cloud frequency difference at altitudes of 7.5 and 12.5 km are presented in Plates 9a and 10a, respectively. At 7.5 km, large enhancements in the frequency difference are shown over the tropical Pacific Ocean, central Chile and Argentina, the central and northwestern Indian Ocean, southeastern Africa, western Australia and adjacent oceans, and the northern midlatitude Atlantic Ocean. Small decreases or no change in cloud occurrence are observed over much of the remaining areas during the 1987 ENSO year. The associated distributions of the standard deviation in cloud frequency during the non-ENSO years are given in Plate 9b. The most interesting features in the distribution are the high standard deviations over the western equatorial Pacific Ocean and Micronesia. Plate 9c

shows that significant changes in cloud frequency occurrence are over the eastern equatorial Pacific Ocean, central South America, the eastern United States, southwestern Africa, the tropical and central Indian Ocean, western Australia and adjacent oceans, and part of the northwestern Pacific Ocean.

At 12.5 km, major geographic areas with increased cloud occurrence include the eastern equatorial Pacific Ocean, the eastern and northern Atlantic Ocean, southern Europe, Russia, Kazakhstan, the Drake Passage between Antarctica and South America, southern Asia, and part of the southern Indian Ocean (Plate 10a). Reduced cloud frequency in 1987 was found over most parts of the extratropical Pacific Ocean, northern Mexico and southern United States, the equatorial Atlantic Ocean, and northwestern Africa (Plate 10a). The standard deviations in clouds frequency for the five non-ENSO years are displayed in Plate 10b. High standard deviations are shown in the equatorial regions centered over Micronesia, the western Indian Ocean, central Africa, northern South America, and the eastern Pacific Ocean. Plate 10c compares the magnitude of the difference in cloud occurrences between the 1987 ENSO year and the mean of the five non-ENSO years with the 5-year cloud variability (Plate 10b). The results suggest that the enhanced cloud occurrences over the eastern equatorial Pacific Ocean, eastern and western Europe, central China, and the southern Indian Ocean are significant at the 95% level.

In a study of the atmospheric temperature change related to the ENSO sea surface temperature (SST) variations, *Reid and Gage* [1993] showed an apparent localized warming taking place just below the tropopause over many tropical stations. This warming is coupled to the lower stratospheric cooling in a dipole-like fashion. *Reid and Gage* suggested that the cause of this particular pattern of temperature response is due to the existence of a large cloud sheet. Presumably, this sheet consists of subvisual cirrus clouds that formed near the tropopause as a result of the increased convective activity during the ENSO event. High-altitude optically thin clouds are known for being capable of blocking upwelling infrared radiation, resulting in significant local warming in the troposphere immediately below and cooling in the lower stratosphere just above [e.g., *Cox*, 1969; *Ackerman et al.*, 1988]. The absence of the dipole temperature variations in some other tropical stations is likely due to the location of these stations in the descending branches of the enhanced large-scale circulation in the tropics. *Reid and Gage* [1993] also suggested that the induced large-scale meridional circulation associated with the intensification of the northern hemisphere subtropical jet stream is probably the mechanism for the observed coldest and highest tropopause during winter. However, the tropical convective activity associated with the onset of the Australian summer monsoon is also a possible cause (see discussion on the STE and dehydration in section 5.5). The forced meridional circulation is such that upward motion occurs on the equatorward side of the jet, and downward motion occurs on the poleward side. The adiabatic cooling induced by the upward motion in the tropical upper troposphere and lower stratosphere as the jet stream strengthens following the onset of winter would raise the tropopause and cause the formation of large-scale subvisual clouds. The enhanced winter tropospheric Hadley circulation and subtropical jet stream have been reported previously during ENSO conditions [*Pan and Oort*, 1983]. Plates 8–10 provide evidence of the enhanced mean circulation during the 1987 ENSO event based on observations from the SAGE II satellite instrument.

6. Summary and Concluding Remarks

A climatology of cloud occurrence frequency has been developed based on the SAGE II observations from 1985 to 1990. The inherent measurement characteristics of the SAGE II instrument allow for partitioning the observed clouds into two categories, i.e., SAGE II measurable clouds and opaque (unmeasurable) clouds. With reference to *Sassen and Cho's* [1992] cloud classifications, the SAGE II measurable clouds are subvisual clouds, and the opaque clouds include all types of clouds except most of the subvisual clouds.

With its high vertical resolution, the derived climatology indicates that subvisual clouds concentrate generally near the tropopause and that the highest frequency, about 70% and 15.5 km, occurs over Micronesia. The zonal mean distributions of the occurrence frequency reflect the characteristics of cloud activities with deep convection in the tropics and with frontal systems at the middle and high latitudes, and general features consistent with the tropospheric mean circulation (Hadley and Ferrel cells) and corresponding seasonal variations. In addition, the altitude-longitude distributions of the cloud occurrence along the equator reveal a pattern that follows the equatorial circulation, including the Walker circulation over the Pacific Ocean. The latitude-longitude distributions of this 6-year cloud climatology exhibit the seasonal expansion and migration behavior of both the subvisual and opaque clouds. This climatology also reveals the intense convective activities during the Indian summer monsoon season even at 17.5-km altitude. In general, the results are very consistent with the cloud climatologies derived from surface observations and other satellite measurements.

The results from a study of the global effect of the 1987 ENSO on cloud occurrence indicate generally enhanced cloud frequency in the tropics and at midlatitudes and reduced cloud frequency in the subtropics and at high latitudes, implying a more intense tropospheric circulation during ENSO years than non-ENSO years. Because the data period of this report covers just one single ENSO event, further studies using data from additional ENSO periods are needed to confirm the present findings. It should be mentioned that unlike the ENSO events during 1982–1983 and 1991–1992, the atmosphere was relatively free from volcanic aerosols during the 1987 ENSO event. Therefore changes in the cloud frequency during the 1987 ENSO event cannot be attributed to volcanic activity.

A study of the seasonal water vapor distribution at 19.5 km, based on SAGE II water vapor measurements, shows that the lowest water vapor mixing ratios (<3 ppmv) are located generally over the same geographic regions as the high SVC occurrence in the tropics. This result provides satellite observational evidence on the connection between stratosphere-troposphere exchange and dehydration processes and high-altitude cloud occurrence important to the dryness of the stratosphere.

In addition to the detection of visible clouds, the capability of the SAGE II instrument to measure optically thin clouds enhances cloud information needed for radiative transfer and climate investigations. A preliminary study indicates that the effects of subvisual clouds on solar and terrestrial radiation

were shown to impact the longwave radiation at the 1 W m^{-2} level with a possible net warming effect (cloud forcing) of 0.5–1 W m^{-2} in the tropics.

The vertical characterization of clouds in the existing climatology typically follows the three-level system, namely, the high-, middle-, and low-level clouds [*World Meteorological Organization*, 1975]. The developed climatology of this investigation inherits the high vertical resolution (1 km) of the SAGE II instrument. Therefore the results derived from the SAGE II solar occultation measurements complement the cloud detection using other techniques such as surface and nadir-viewing satellite observations. The numerical data presented in this report are available to readers by ftp: ftp *arhs1.larc.nasa.gov*, username > *anonymous*, password > enter user ID as password, ftp > *cd pub/Sage2cc*.

Finally, the SAGE II cloud data have been compared with the ISCCP results by *Liao et al.* [1995a]. Also, some SAGE II cloud data comparison analyses can be found in the report by *Chiou et al.* [1990] and in the paper by *Wang et al.* [1995b]. However, a detailed comparison study using all available cloud data sets is still missing. An investigation of this type would be very useful for understanding the current cloud data sets that have been derived from various retrieval algorithms. It would make the full range of data more valuable for use in climate model verification and improvement.

Acknowledgment. The authors are grateful to Thomas P. Charlock of NASA Langley Research Center for many helpful discussions. This study is supported by NASA contracts NAS1-19603, NAS1-19976, and NAS1-18941.

References

Ackerman, T. P., K.-N. Liou, F. P. J. Valero, and L. Pfister, Heating rates in tropical anvils, *J. Atmos. Sci., 45*, 1606–1623, 1988.

Ansmann, A., et al., Measurements with a ground-based lidar network during ICE '80, in *Optical Remote Sensing of the Atmosphere*, conference edition, Opt. Soc. Am., Washington, D.C., 1991.

Chahine, M. T., The hydrological cycle and its influence on climate, *Nature, 359*, 373–380, 1992.

Chiou, E. W., M. P. McCormick, W. P. Chu, and G. Y. Yue, Global distributions of cirrus determined from SAGE II occultation measurements between November 1984 and October 1988, in *Conference on Cloud Physics*, pp. 513–516, Am. Meteorol. Soc., Boston, Mass., 1990.

Chu, W. P., M. P. McCormick, J. Lenoble, C. Brogniez, and P. Pruvost, SAGE II inversion algorithm, *J. Geophys. Res., 94*, 8339–8351, 1989.

Chu, W. P., E. W. Chiou, J. C. Larsen, L. W. Thomason, D. Rind, J. J. Buglia, S. Oltmans, M. P. McCormick, and L. M. McMaster, Algorithms and sensitivity analyses for Stratospheric Aerosol and Gas Experiment II water vapor retrieval, *J. Geophys. Res., 98*, 4857–4866, 1993.

Cox, S. K., Observational evidence of anomalous infrared cooling in a clear tropical atmosphere, *J. Atmos. Sci., 26*, 1347–1349, 1969.

Cox, S. K., D. S. McDougal, D. A. Randall, and R. A. Schiffer, FIRE—The first ISCCP regional experiment, *Bull. Am. Meteorol. Soc., 68*, 114–118, 1987.

Danielsen, E. F., A dehydration mechanism for the stratosphere, *Geophys. Res. Lett., 9*, 605–608, 1982a.

Danielsen, E. F., Statistics of cold cumulonimbus anvils based on enhanced infrared photographs, *Geophys. Res. Lett., 9*, 601–604, 1982b.

Danielsen, E. F., In situ evidence of rapid, vertical, irreversible transport of lower tropospheric air into the lower tropical stratosphere by convective cloud turrets and by large-scale upwelling in tropical cyclones, *J. Geophys. Res., 98*, 8665–8681, 1993.

Fu, Q., and K.-N. Liou, Parameterization of the radiative properties of cirrus clouds, *J. Atmos. Sci., 50*, 2008–2025, 1994.

Gayet, J. F., How accurately can we measure cirrus cloud microphysical properties?, in *Proceedings of the World Meteorological Organization Workshop on Cloud Microphysics and Applications to Global Change, WMO/TD 537*, pp. 169–173, Geneva, 1992.

Heymsfield, A. J., Microphysical structure of stratiform and cirrus clouds, in *Aerosol-Cloud-Climate Interactions*, edited by P. V. Hobbs, pp. 97–121, Academic, San Diego, Calif., 1993.

Hobbs, P. V. (Ed.), *Aerosol-Cloud-Climate Interactions*, 233 pp., Academic, San Diego, Calif., 1993.

Holton, J. R., On the global exchange of mass between the stratosphere and troposphere, *J. Atmos. Sci., 47*, 392–395, 1990.

Holton, J. R., P. H. Haynes, M. E. McIntyre, A. R. Douglass, R. B. Rood, and L. Pfister, Stratosphere-troposphere exchange, *Rev. Geophys., 33*, 403–439, 1995.

Kent, G. S., D. M. Winker, M. T. Osborn, and K. M. Skeens, A model for the separation of cloud and aerosol in SAGE II occultation data, *J. Geophys. Res., 98*, 20,725–20,735, 1993.

Kent, G. S., E. R. Williams, P.-H. Wang, M. P. McCormick, and K. M. Skeens, Surface temperature related variations in tropical cirrus cloud as measured by SAGE II, *J. Clim., 8*, 2577–2594, 1995a.

Kent, G. S., P.-H. Wang, M. P. McCormick, and K. M. Skeens, Multiyear SAGE II measurements of upper tropospheric aerosol characteristics, *J. Geophys. Res., 100*, 13,875–13,899, 1995b.

Kley, D., A. L. Schmeltekopf, K. Kelly, R. H. Winkler, T. L. Thompson, and M. McFarland, Transport of water through the tropical tropopause, *Geophys. Res. Lett., 9*, 617–620, 1982.

Knollenberg, R. G., K. Kelly, and J. C. Wilson, Measurements of high number densities of ice crystals in the tops of tropical cumulonimbus, *J. Geophys. Res., 98*, 8639–8664, 1993.

Lau, K.-M., and P. J. Sheu, Teleconnections in global rainfall anomalies: Seasonal to inter-decadal time scales, in *Teleconnections Linking Worldwide Climate Anomalies*, edited by M.H. Glantz et al., pp. 227–256, Cambridge Univ. Press, New York, 1991.

Liao, X., W. B. Rossow, and D. Rind, Comparison between SAGE II and ISCCP high-level clouds, 2, Locating cloud tops, *J. Geophys. Res., 100*, 1137–1147, 1995a.

Liao, X., W. B. Rossow, and D. Rind, Comparison between SAGE II and ISCCP high-level clouds, 1, Global and zonal mean cloud amounts, *J. Geophys. Res., 100*, 1121–1135, 1995b.

Liou, K. N., *Radiation and Cloud Processes in the Atmosphere*, 487 pp., Oxford Univ. Press, New York, 1992.

Manabe, S., J. Smagorinsky, and R. F. Strickler, Simulated climatology of a general circulation model with a hydrological cycle, *Mon. Weather Rev., 93*, 769–798, 1965.

Mauldin, L. E., III, N. H. Zaun, M. P. McCormick, J. H. Guy, and W. R. Vaughn, Stratospheric Aerosol and Gas Experiment II instrument: A functional description, *Opt. Eng., 24*, 307–312, 1985.

McCormick, M. P., SAGE II: An overview, *Adv. Space Res., 7*, 319–326, 1987.

McCormick, M. P., Initial assessment of the stratospheric and climatic impact of the 1991 Mount Pinatubo eruption: Prologue, *Geophys. Res. Lett., 9*, 149, 1992.

McCormick, M. P., P.-H. Wang, and L. R. Poole, Stratospheric aerosols and clouds, in *Aerosol-Cloud-Climate Interactions*, edited by P. Hobbs, pp. 205–222, Academic, San Diego, Calif., 1993.

McCormick, M. P., L. W. Thomason, and C. R. Trepte, Atmospheric effects of the Mount Pinatubo eruption, *Nature, 373*, 399–404, 1995.

Menzies, R. T., and D. M. Tratt, Evidence of seasonally dependent stratosphere-troposphere exchange and purging of lower stratospheric aerosol from a multiyear lidar data set, *J. Geophys. Res., 100*, 3139–3148, 1995.

Minnis, P., and E. F. Harrison, Diurnal variability of regional cloud and clear-sky radiative parameters derived from GOES data, II, November 1978 cloud distributions, *J. Clim. Appl. Meteorol., 23*, 1012–1031, 1984.

Minnis, P., E. F. Harrison, L. L. Stowe, G. G. Gibson, F. M. Denn, D. R. Doelling, and W. L. Smith Jr., Radiative climate forcing by the Mount Pinatubo eruption, *Science, 259*, 1411–1415, 1993.

Mote, P. W., K. H. Rosenlof, M. E. McIntyre, E. S. Carr, J. C. Gille, J. R. Holton, J. S. Kinnersley, H. C. Pumphrey, J. M. Russell III, and J. W. Waters, An atmospheric tape recorder: The imprint of tropical tropopause temperatures on stratospheric water vapor, *J. Geophys. Res., 101*, 3989–4006, 1996.

National Oceanic and Atmospheric Administration, *Climate Diagnostics Bulletin: June 1995*, Clim. Anal. Cent., U.S. Dep. of Commer., Washington, D. C., 1995.

Newell R. E., and S. Gould-Stewart, A stratospheric fountain, *J. Atmos. Sci., 38*, 2789–2796, 1981.

Oort, A. H., Global atmospheric circulation statistics, 1958–1973, *NOAA Prof. Pap., 14*, 180 pp., 1983.

Pan, Y. H., and A. H. Oort, Global climate variations connected with sea surface temperature anomalies in the eastern equatorial Pacific Ocean for the 1958–73 period, *Mon. Weather Rev., 111*, 1244–1258, 1983.

Peixoto, J. P., and A. H. Oort, *Physics of Climate*, 520 pp., Am. Inst. of Phys., New York, 1992.

Platt, C. M., et al., The experimental cloud lidar pilot study (ECLIPS) for cloud-radiation research, *Bull. Am. Meteorol. Soc., 75*, 1635–1654, 1994.

Ramanathan, V., R. D. Cess, E. F. Harrison, P. Minnis, B. R. Barkstrom, E. Ahmad, and D. Hartmann, Cloud-radiative forcing and climate: Results from the Earth Radiation Budget Experiment, *Science, 243*, 57–63, 1989.

Reid, G. C., and K. S. Gage, Troposphere-stratosphere coupling in the tropics: The role of El Niño and the QBO, in *The Role of the Stratosphere in Global Change*, edited by M.-L. Chanin, *NATO ASI Ser.*, pp. 245–266, Springer-Verlag, New York, 1993.

Rossow, W. B., and R. A. Schiffer, ISCCP cloud data products, *Bull. Am. Meteorol. Soc., 72*, 2–20, 1991.

Russell, P. B., L. Pfister, and H. B. Selkirk, The tropical experiment of the Stratosphere-Troposphere Exchange Project (STEP): Science objectives, operations, and summary findings, *J. Geophys. Res., 98*, 8563–8589, 1993.

Sassen, K., and B. S. Cho, Subvisual-thin cirrus lidar dataset for satellite verification and climatological research, *J. Appl. Meteorol., 31*, 1275–1285, 1992.

Sassen, K., A. J. Heymsfield, and D. Starr, Is there a cirrus small particle anomaly?, in *Conference on Cloud Physics*, Am. Meteorol. Soc., pp. J91–J95, Boston, Mass., 1990.

Schiffer, R. A., and W. B. Rossow, ISCCP global radiance data set: A new resource for climate research, *Bull. Am. Meteorol. Soc., 66*, 779–784, 1985.

Stowe, L. L., H. Y. M. Yeh, T. F. Eck, C. G. Wellemeyer, and H. L. Kyle, Nimbus-7 global cloud climatology, II, First year results, *J. Clim., 2*, 671–709, 1989.

Von de Berg, L., A. Pyomjamsri, and J. Schmets, Monthly mean upper tropospheric humidities in cloud-free area from Meteosat observations, *Int. J. Climatol., 11*, 11,819–11,836, 1991.

Wang, P.-H., SAGE II tropospheric measurement frequency and its meteorological implication, in *Seventh Conference on Satellite Meteorology and Oceanography*, pp. J15–J18, Am. Meteorol. Soc., Boston, Mass., 1994.

Wang, P.-H., M. P. McCormick, L. R. Poole, W. P. Chu, G. K. Yue, G. S. Kent, and K. M. Skeens, Tropical high cloud characteristics derived from SAGE II extinction measurements, *Atmos. Res., 34*, 53–83, 1994a.

Wang, P.-H., M. P. McCormick, G. S. Kent, and L. Thomason, SAGE II long-term measurements of stratospheric and upper tropospheric aerosols, in *Atmospheric Sensing and Modeling*, vol. 2311, edited by R. P. Santer, pp. 2–9, SPIE—Int. Soc. for Opt. Eng., Bellingham, Wash., 1994b.

Wang, P.-H., P. Minnis, and G. K. Yue, Extinction coefficient (1 μm) properties of high-altitude clouds from solar occultation measurements (1985–1990): Evidence of volcanic aerosol effect, *J. Geophys. Res., 100*, 3181–3199, 1995a.

Wang, P.-H., M. P. McCormick, P. Minnis, G. S. Kent, G. K. Yue, and K. M. Skeens, A method for estimating vertical distribution of the SAGE II opaque cloud frequency, *Geophys. Res. Lett., 22*, 243–246, 1995b.

Warren, S. G., C. J. Hahn, J. London, R. M. Chervin, and R. L. Jenne, Global distribution of total cloud cover and cloud type amounts over land, *NCAR TN-273+STR*, Natl. Cent. for Atmos. Res., Boulder, Colo., 1986. (Available as DE87-006903 from Natl. Tech. Inf. Serv., Springfield, VA.

Warren, S. G., C. J. Hahn, J. London, R. M. Chervin, and R. L. Jenne, Global distribution of total cloud cover and cloud type amounts over ocean, *NCAR TN-317+STR*, Natl. Cent. For Atmos. Res., Boulder, Colo., 1988.

Woodbury, G. E., and M. P. McCormick, Global distributions of cirrus clouds determined from SAGE data, *Geophys. Res. Lett., 10*, 1180–1183, 1983.

Woodbury, G. E., and M. P. McCormick, Zonal and geographical distributions of cirrus clouds determined from SAGE data, *J. Geophys. Res., 91*, 2775–2785, 1986.

World Meteorological Organization (WMO), *International Cloud Atlas*, vol. I, *Manual on the Observation of Clouds and Other Meteors*, Geneva, 1975.

WMO, An experimental cloud lidar pilot study (ECLIPS), report of the WCRP/CSIRO workshop on cloud base measurement, *WMO/TD, 251*, Geneva, 1988.

Wylie, D. P., W. P. Menzel, H. M. Woolf, and K. I. Strabala, Four years of global cirrus cloud statistics using HIRS, *J. Clim., 7*, 1972–1986, 1994.

Zhang, C., On the annual cycle in highest, coldest clouds in the tropics, *J. Clim., 6*, 1987–1990, 1993.

G. S. Kent, K. M. Skeens, and P-H. Wang, Science and Technology Corporation, 101 Research Drive, Hampton, VA 23666-1340. (e-mail: kent@arbs9.larc.nasa.gov; kristi@arbs4.larc.nasa.gov; wang@arbs3.larc.nasa.gov)

P. Minnis, Atmospheric Science Division, NASA Langley Research Center, Mail Stop 420, Hampton, VA 23681-0001. (e-mail: p.minnis@larc.nasa.gov)

M. P. McCormick, Department of Physics, Hampton University, Hampton, VA 23668-5439. (e-mail: mccormic@gprc.hamptonu.edu)

(Received October 27, 1995, revised May 21, 1996; accepted May 21, 1996.)